ESAIM: M2AN 60 (2026) 1269–1295
https://doi.org/10.1051/m2an/2026036

ESAIM: Mathematical Modelling and Numerical Analysis
www.esaim-m2an.org

ELLIPTIC INTERFACE PROBLEM APPROXIMATED BY CUTFEM: I. FLUX RECOVERY AND NUMERICAL VALIDATION OF ADAPTIVE MESH REFINEMENT

Daniela Capatina[1,*], Aimene Gouasmi[1] and Cuiyu He[2]

Abstract. We study an elliptic interface problem with discontinuous diffusion coefficients on unfitted meshes using the CutFEM method. Our main contribution is the reconstruction of an element-wise conservative flux from the CutFEM solution and its use in *a posteriori* error estimation. We introduce a hybrid mixed formulation with locally computable Lagrange multipliers and reconstruct a flux in the immersed Raviart–Thomas space. Based on this, we propose a new *a posteriori* error estimator that includes both volume and interface terms. We state here its robust reliability and local efficiency, which are proved in Part II of this work. The approach is validated through numerical experiments.

Mathematics Subject Classification. 65N15, 65N30, 65N50.

Received July 11, 2025. Accepted April 13, 2026.

1. Introduction

Local reconstruction of conservative fluxes from finite element solutions plays a key role in applications such as *a posteriori* error estimation [1, 4, 5, 9, 10, 16, 27] and enforcing flux conservation in continuum mechanics [17, 25, 29]. These techniques are essential for accurately representing physical fluxes – such as heat, mass, or momentum – in solid mechanics and porous media.

In this work, we consider an elliptic problem with an interface that is not aligned with the finite element mesh, characterized by discontinuous diffusion coefficients and standard transmission conditions at the interface; we allow for a jump in the normal flux across the interface. We use the CutFEM method (cf. [7, 8]) to solve the interface problem – a Nitsche type formulation that is robust with respect to discretization, diffusion contrasts, and mesh/interface geometry, owing to the inclusion of additional stabilization terms.

Our goal is to reconstruct conservative fluxes and employ them in *a posteriori* error analysis and adaptive mesh refinement. To the best of our knowledge, these topics remain largely unexplored in the context of CutFEM. While conservative flux reconstruction for CutFEM solutions has been investigated in [12] for Poisson boundary problems on unfitted meshes, no such developments exist for interface problems.

Keywords and phrases. Elliptic interface problem, CutFEM, conservative flux reconstruction, *a posteriori* error estimation, adaptive finite element methods, immersed Raviart–Thomas elements.

[1] LMAP CNRS UMR 5142, University of Pau and Pays de l'Adour, 64013 Pau, France.
[2] The University of Georgia, Athens, GA 30602, USA.
*Corresponding author: daniela.capatina@univ-pau.fr

Regarding the reconstruction method, we have chosen to generalize an approach previously developed for the Poisson problem in [2] and then extended to diffusion problems in [13]. The key idea is to introduce a hybrid mixed formulation whose primal solution is equivalent to the discrete CutFEM solution, while also incorporating an additional Lagrange multiplier defined on mesh edges to correct the normal trace of the flux. A different hybrid mixed formulation was considered in [14], in which the Lagrange multiplier approximates the trace of the solution u. It should be noted that we do not solve any mixed problem for the reconstruction, contrary to other existing techniques such as [28]. The Lagrange multiplier can be computed locally on element patches.

The extension of the approach developed in [2, 13] to elliptic interface problems using CutFEM on unfitted meshes raises several important questions.

The first question concerns the well-posedness of the hybrid mixed formulation. To ensure the stability, convergence, and robustness of the numerical method, the constants involved in the analysis ideally should be independent of the discretization parameters, the diffusion coefficients, and the mesh/interface geometry. Following the approach in [13] for fitted meshes, we propose a mixed formulation with Lagrange multipliers assigned separately to the edges within each individual subdomain. In the case of cut elements, this results in two distinct multipliers defined over each cut edge that has non-zero intersections with all subdomains. We demonstrate that the mixed formulation possesses several key properties: its primal solution is equivalent to the original discrete CutFEM solution, it is fully robust with respect to both numerical and physical parameters, and it allows the multipliers to be computed locally.

The second question concerns the reconstruction of numerical fluxes in cells cut by the interface, where appropriate notions of discrete conservation and transmission conditions must be defined. Although multiple definitions of fluxes are possible, this issue is closely tied to a third question: the development of *a posteriori* error estimators based on equilibrated fluxes. We propose a global error estimator consisting of two parts: a standard term – the weighted L^2-norm of the difference between the equilibrated and numerical fluxes – and a new interface term that accounts for discontinuities in the approximate solution across Γ. The main challenge lies in proving both the (sharp) reliability and the local efficiency of the estimator, with constants that remain robust with respect to the diffusion coefficients and the mesh-interface configuration.

To enforce both element-wise conservation and normal trace continuity in the cut cells, we define a unique flux σ_h satisfying $[\sigma_h \cdot n_\Gamma] = 0$ across the interface Γ and $\operatorname{div} \sigma_h = -f_h$. The Lagrange multipliers introduced earlier serve to correct the normal trace of the numerical flux from the CutFEM solution. For the sake of local efficiency in the *a posteriori* error analysis, the flux reconstruction is performed in the immersed Raviart–Thomas space recently introduced in [22].

The immersed finite element (IFE) method [23] aims to modify traditional finite element spaces in order to recover optimal approximation capabilities on unfitted meshes. Notably, the IFE method retains the same degrees of freedom as traditional finite element methods and can revert to the conventional finite element method when the interface is absent. This characteristic, where IFE spaces are isomorphic to standard finite element spaces defined on the same mesh, is particularly beneficial for problems involving moving interfaces [21].

The lowest-order immersed Raviart–Thomas space $\mathcal{IRT}^0$ [21, 22] was developed to handle unfitted meshes by modifying standard Raviart–Thomas functions [26] to maintain optimal approximation properties on cut elements. Functions in $\mathcal{IRT}^0$ are piecewise $\mathcal{RT}^0$, enforce strong continuity of the normal trace across the interface, and incorporate weak continuity of tangential flux. However, they only satisfy weak continuity on cut edges, and thus $\mathcal{IRT}^0$ is not conforming in $H(\operatorname{div}, \Omega)$, which introduces an additional *a posteriori* error term on the cut edges. The method also accommodates non-homogeneous transmission conditions.

A detailed theoretical analysis – presented in [11] – establishes the reliability and local efficiency of the proposed *a posteriori* error estimator. The associated constants are independent of the diffusion coefficients and the mesh/interface configuration for reliability, and depend explicitly on these parameters for local efficiency. In the present paper, we summarize the main results of this analysis and validate them through numerical experiments.

The paper is organized as follows. The model problem and relevant notation are introduced in Section 2. Section 3 presents the finite element discretization on unfitted meshes using CutFEM and sets the foundation

for flux recovery *via* an equivalent mixed formulation with locally computable Lagrange multipliers. In Section 4, we describe the local flux reconstruction in the immersed Raviart–Thomas space and establish the element-wise conservation property. Section 5 applies the reconstructed fluxes to the *a posteriori* error analysis, where we define error estimators and state without proof their sharp reliability and local efficiency. Section 6 reports several numerical experiments that confirm the theoretical results. The paper concludes with an appendix detailing the numerical implementation of the immersed Raviart–Thomas space.

2. The continuous problem and notation

Let Ω be a 2D polygonal domain and Γ a Lipschitz continuous, piecewise smooth interface separating Ω into two disjoint subdomains: $\bar{\Omega} = \bar{\Omega}^1 \cup \bar{\Omega}^2$, $\partial\Omega^1 \cap \partial\Omega^2 = \Gamma$. We denote by n_Γ the unit normal vector to Γ oriented from Ω^1 to Ω^2. We consider the following model problem:

$$\begin{cases} -div(K\nabla u) = f & \text{in } \Omega^i \ (i=1,2), \\ u = 0 & \text{on } \partial\Omega \\ [u] = 0,\ [K\nabla u \cdot n_\Gamma] = g & \text{on } \Gamma. \end{cases} \tag{1}$$

The jumps across Γ are given by

$$[u] = u_1 - u_2, \quad [K\nabla u \cdot n_\Gamma] = (K_1\nabla u_1 - K_2\nabla u_2)\cdot n_\Gamma,$$

where $u_{|\Omega^i} = u_i$ and $K_{|\Omega^i} = K_i$, for $i = 1, 2$. We suppose $f \in L^2(\Omega)$, $g \in L^2(\Gamma)$ and, for the sake of simplicity, here we assume $K_i = k_i I$ with $k_i > 0$, for $i = 1, 2$. The approach can be extended to piecewise constant positive definite tensors K and to other boundary conditions on $\partial\Omega$.

We consider the following weak formulation of problem (1), which clearly has a unique solution: Find $u \in H^1_0(\Omega)$ such that

$$\int_\Omega K\nabla u \cdot \nabla v \,\mathrm{d}x = \int_\Omega fv \,\mathrm{d}x + \int_\Gamma gv \,\mathrm{d}s \quad \forall v \in H^1_0(\Omega). \tag{2}$$

We next introduce some notation for the finite element approximation of (2). Let $\mathcal{T}_h$ denote a regular triangular mesh of Ω, whose elements are closed sets, and $\mathcal{F}_h$ be the set of edges. The diameter of $T \in \mathcal{T}_h$ (and the length of $F \in \mathcal{F}_h$) is denoted h_T (and h_F). For an interior edge F, n_F is a fixed unit normal vector to F, oriented from T_F^- to T_F^+, where T_F^- and T_F^+ are the two triangles that share F, see Figure 1. If $F \subset \partial\Omega$, then n_F is the outward normal vector to Ω while if $F \subset \Gamma$, then $n_F = n_\Gamma$. For $\omega \subset \mathbb{R}^d$ with $d = 1, 2$, we denote the $L^2(\omega)$-norm by $\|\cdot\|_\omega$ and the $L^2(\omega)$-orthogonal projection onto $P^m(\omega)$ by π^m_ω, for $m \in \mathbb{N}$, where $P^m(\omega)$ denotes the space of polynomials of degree m restricted to ω. For $i = 1, 2$, we define:

$$\mathcal{T}_h^i = \left\{T \in \mathcal{T}_h \ ;\ T \cap \Omega^i \neq \emptyset\right\}, \quad \mathcal{F}_h^i = \left\{F \in \mathcal{F}_h \ ;\ F \cap \Omega^i \neq \emptyset\right\}$$

and we set $\Omega_h^i = \bigcup_{T\in\mathcal{T}_h^i} T$; note that $\Omega^i \subset \Omega_h^i$. Let also $\mathcal{N}_h^i$ be the set of nodes belonging to Ω_h^i. As regards the cut elements, let:

$$\begin{aligned} &\mathcal{T}_h^\Gamma = \left\{T \in \mathcal{T}_h \ ;\ T \cap \Gamma \neq \emptyset\right\}, \quad \mathcal{F}_h^\Gamma = \left\{F \in \mathcal{F}_h \ ;\ F \cap \Gamma \neq \emptyset\right\}, \\ &\mathcal{F}_g^i = \left\{F \in \mathcal{F}_h^i;\ (T_F^+ \cup T_F^-) \cap \Gamma \neq \emptyset\right\}, \quad T^i = T \cap \Omega^i \ \ \forall T \in \mathcal{T}_h^\Gamma, \quad F^i = F \cap \Omega^i \ \ \forall F \in \mathcal{F}_h^\Gamma, \quad (i = 1, 2). \end{aligned}$$

In order to focus on flux reconstruction, we assume here that Γ is a polygonal line such that for each $T \in \mathcal{T}_h^\Gamma$, the intersection $\Gamma_T := T \cap \Gamma$ is a line segment. For a function $v \in L^2(\Omega)$, sufficiently smooth on each Ω^i but discontinuous across Γ, we define the two following means at a point $x \in \Gamma$:

$$\{v\}(x) = \omega_1 v_1(x) + \omega_2 v_2(x), \quad \{v\}^*(x) = \omega_2 v_1(x) + \omega_1 v_2(x),$$

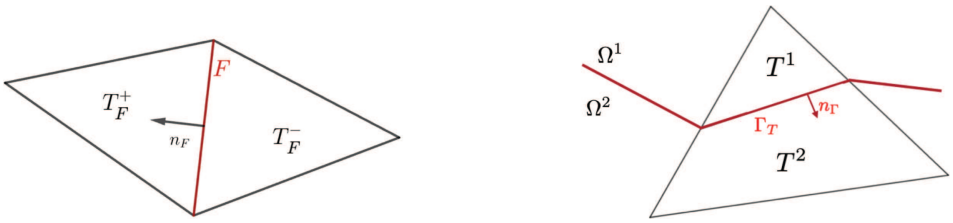

FIGURE 1. $T_F^{\pm}$ with respect to n_F (*left*) and $T^{1,2}$ with respect to n_Γ (*right*).

where the weights ω_1, ω_2 are given (cf. [18]) by:

$$\omega_1 = \frac{k_2}{k_2 + k_1}, \quad \omega_2 = \frac{k_1}{k_1 + k_2}.$$

It is also useful to introduce the harmonic mean $k_\Gamma = k_1 k_2/(k_1 + k_2)$.

Furthermore, we introduce the arithmetic mean and the jump across an interior edge $F \in \mathcal{F}_h^i$, for $1 \leq i \leq 2$, as follows:

$$\langle v \rangle = \frac{1}{2}(v^- + v^+), \quad [\![v]\!] = v^- - v^+, \quad [\![\partial_n v]\!] = [\![\nabla v]\!] \cdot n_F.$$

For boundary edges, we set $\langle v \rangle = [\![v]\!] = v$. Finally, for $i = 1, 2$, let

$$V^i = \left\{ v \in H^1(\Omega_h^i) \ ; \ v_{|(\partial\Omega^i \setminus \Gamma)} = 0 \right\}.$$

We use the symbols $\gtrsim$ and $\lesssim$ to indicate the existence of a generic constant that is independent of the mesh size, the interface geometry and the diffusion coefficients; such a constant may depend on the shape regularity of the mesh, and possibly on an upper bound for the stabilisation parameters γ and γ_g.

3. The CutFEM approximation

In the numerical approximation of (2), the transmission conditions on Γ are taken into account by means of Nitsche's method [24]. Moreover, we use CutFEM [7] to stabilize the approach with respect to the geometry of the interface, by adding a ghost penalty term.

3.1. Primal discrete formulation

We consider the discrete space $\mathcal{C}_h = \mathcal{C}_h^1 \times \mathcal{C}_h^2$, where for $1 \leq i \leq 2$,

$$\mathcal{C}_h^i = \left\{ v \in V^i : \ v_{|T} \in P^1(T), \ \forall \ T \in \mathcal{T}_h^i \right\}.$$

Note that the degrees of freedom on the cut cells are doubled. We define the following bilinear and linear forms: for $u_h = (u_{h,1}, u_{h,2}) \in \mathcal{C}_h$ and $v_h = (v_{h,1}, v_{h,2}) \in \mathcal{C}_h$, let

$$a_i(u_{h,i}, v_{h,i}) = \sum_{T \in \mathcal{T}_h^i} \int_{T^i} k_i \nabla u_{h,i} \cdot \nabla v_{h,i} \, \mathrm{d}x = \int_{\Omega^i} k_i \nabla u_{h,i} \cdot \nabla v_{h,i} \, \mathrm{d}x \quad (i = 1, 2),$$

$$j_i(u_{h,i}, v_{h,i}) = \sum_{F \in \mathcal{F}_g^i} h_F \int_F k_i [\![\partial_n u_{h,i}]\!][\![\partial_n v_{h,i}]\!] \, \mathrm{d}s \quad (i = 1, 2),$$

$$a_\Gamma(u_h, v_h) = \sum_{T \in \mathcal{T}_h^\Gamma} \int_{\Gamma_T} \left(\frac{\gamma k_\Gamma}{h_T} [u_h][v_h] - \{K \nabla u_h \cdot n_\Gamma\}[v_h] - \{K \nabla v_h \cdot n_\Gamma\}[u_h] \right) \mathrm{d}s,$$

$$l_h(v_h) = \sum_{i=1}^{2} \int_{\Omega^i} f v_{h,i} \, \mathrm{d}x + \sum_{T \in \mathcal{T}_h^\Gamma} \int_{\Gamma_T} g \{v_h\}^* \, \mathrm{d}s.$$

Here above, $a_i(\cdot,\cdot)$ and $j_i(\cdot,\cdot)$ represent the main part and the ghost penalty term, respectively, whereas the remaining form $a_\Gamma(\cdot\cdot)$ takes into account the terms which result from the integration by parts, the symmetrization and the Nitsche stabilization. The discrete problem then reads: Find $u_h = (u_{h,1}, u_{h,2}) \in \mathcal{C}_h$ such that

$$a_h(u_h, v_h) = l_h(v_h) \quad \forall v_h \in \mathcal{C}_h, \tag{3}$$

where

$$a_h(u_h, v_h) = \sum_{i=1}^{2} \Big(a_i(u_{h,i}, v_{h,i}) + \gamma_g j_i(u_{h,i}, v_{h,i}) \Big) + a_\Gamma(u_h, v_h).$$

It is known (cf. [7]) that the stabilization parameters $\gamma > 0$ and $\gamma_g > 0$ can be chosen independently of the mesh, the interface geometry and the diffusion coefficients.

For any $v_h \in \mathcal{C}_h$, we define the norm:

$$\|v_h\|_h^2 = \sum_{i=1}^{2} \Big(\|k_i^{1/2} \nabla v_{h,i}\|_{\Omega^i}^2 + j_i(v_{h,i}, v_{h,i}) \Big) + \sum_{T \in \mathcal{T}_h^\Gamma} \int_{\Gamma_T} \frac{k_\Gamma}{h_T} [v_h]^2 \, \mathrm{d}s.$$

It is well-known that for γ large enough, the bilinear form $a_h(\cdot,\cdot)$ is uniformly $(\mathcal{C}_h, \|\cdot\|_h)$-coercive. To establish this result, two lemmas are required.

Lemma 3.1 (Trace inequality)**.** *There exists a constant $C_\Gamma > 0$ independent of the mesh/interface geometry such that for any $T \in \mathcal{T}_h^\Gamma$ and any $v \in H^1(T)$,*

$$\|v\|_{\Gamma_T}^2 \le C_\Gamma \Big(h_T^{-1} \|v\|_T^2 + h_T \|\nabla v\|_T^2 \Big). \tag{4}$$

Lemma 3.2. *There exists a constant $C_g > 0$ independent of the mesh-interface intersection for positive parameter γ_g, such that, for any $v_{h,i} \in \mathcal{C}_h^i$ $(i = 1, 2)$,*

$$C_g \|k_i^{1/2} \nabla v_{h,i}\|_{\Omega_h^i}^2 \le \|k_i^{1/2} \nabla v_{h,i}\|_{\Omega^i}^2 + \gamma_g j_i(v_{h,i}, v_{h,i}).$$

For the proof, we refer the reader to [8]. Thanks to the Lax-Milgram theorem, the problem (3) has a unique solution. The following *a priori* error estimate is also known [8].

Theorem 3.3. *Let u_h be the CutFEM solution of (3) and u the solution of (2). Assume that $u_{|\Omega^i} \in H^{1+\varepsilon}(\Omega^i)$, where $\varepsilon > 0$. Then, there exists a constant $C > 0$ independent of the mesh size $h = \max_{T \in \mathcal{T}_h} h_T$ and the mesh/interface configuration but depending on the diffusion coefficients such that:*

$$\sum_{i=1}^{2} \|u - u_{h,i}\|_{H^1(\Omega^i)} \le C h^\varepsilon \sum_{i=1}^{2} \|u\|_{H^{1+\varepsilon}(\Omega^i)}.$$

The method can also accomodate a nonhomogeneous jump condition $[u] = \chi$ on Γ, where $\chi \in H^{1/2}(\Gamma)$. Its treatment is analogous to that of a non-homogeneous Dirichlet condition by Nitsche's method, and it consists in adding to the linear form $l_h(\cdot)$ the term $\sum_{T \in \mathcal{T}^\Gamma} \int_{\Gamma_T} \Big(\frac{\gamma k_\Gamma}{h_T} [v_h] - \{K \nabla v_h \cdot n_\Gamma\} \Big) \chi \, \mathrm{d}s$.

3.2. Equivalent mixed formulation

In the sequel, we aim to construct, for $i \in \{1, 2\}$, discrete functions $\theta_{h,i}$ living on the interior edges of the subdomains Ω_h^i. These functions, which will serve to correct the normal flux, are introduced, following [2], as the Lagrange multipliers of a hybrid mixed formulation whose primal solution coincides with u_h. In the CutFEM context where one deals with cut edges, it is important to note that the multipliers are defined on the whole

edges, in order to avoid the use of sub-edges which could be small. We thus employ standard finite element spaces on the whole elements.

In order to introduce an equivalent mixed formulation of (3), we define the following finite-dimensional spaces:

$$\mathcal{D}_h = \mathcal{D}_h^1 \times \mathcal{D}_h^2, \quad \mathcal{M}_h = \mathcal{M}_h^1 \times \mathcal{M}_h^2,$$

where for $i = 1, 2$ we set:

$$\mathcal{D}_h^i = \{v \in L^2(\mathcal{T}_h^i);\ v_{|T} \in P^1(T)\ \forall T \in \mathcal{T}_h^i\},$$
$$\mathcal{M}_h^i = \left\{\mu \in L^2(\mathcal{F}_h^i);\ \mu|_F \in P^1(F)\ \forall F \in \mathcal{F}_h^i,\ \sum_{F \in \mathcal{F}_N} \mathfrak{s}_N^F h_F \mu_{|F}(N) = 0 \quad \forall N \in \overset{\circ}{\mathcal{N}}{}_h^i\right\}.$$

Here above, $\overset{\circ}{\mathcal{N}}{}_h^i$ denotes the set of nodes interior to Ω_h^i, $\mathcal{F}_N$ the set of edges sharing the node N, and $\mathfrak{s}_N^F = \mathrm{sign}(n_F, N)$ is equal to $1(-1)$ if the orientation of n_F with respect to the node N is in the clockwise (counter-clockwise) rotation. We endow these spaces with the following norms:

$$\|v_h\|_{\mathcal{D}_h}^2 = \|v_h\|_h^2 + \sum_{i=1}^{2} \sum_{F \in \mathcal{F}_h^i} h_F^{-1} \int_F k_i [\![v_{h,i}]\!]^2 \, \mathrm{d}s, \qquad \forall v_h = (v_{h,1}, v_{h,2}) \in \mathcal{D}_h,$$

$$\|\mu_h\|_{\mathcal{M}_h}^2 = \sum_{i=1}^{2} \sum_{F \in \mathcal{F}_h^i} h_F \int_F k_i (\mu_{h,i})^2 \, \mathrm{d}s, \qquad \forall \mu_h = (\mu_{h,1}, \mu_{h,2}) \in \mathcal{M}_h.$$

We next consider the mixed formulation: Find $(\tilde{u}_h, \theta_h) \in \mathcal{D}_h \times \mathcal{M}_h$, such that

$$\begin{aligned} \tilde{a}_h(\tilde{u}_h, v_h) + b_h(\theta_h, v_h) &= l_h(v_h) \qquad \forall v_h \in \mathcal{D}_h, \\ b_h(\mu_h, \tilde{u}_h) &= 0 \qquad \forall \mu_h \in \mathcal{M}_h, \end{aligned} \tag{5}$$

where

$$\tilde{a}_h(\cdot,\cdot) = a_h(\cdot,\cdot) - d_h(\cdot,\cdot), \quad b_h(\mu_h, v_h) = \sum_{i=1}^{2} b_{h,i}(\mu_{h,i}, v_{h,i}),$$

$$d_h(\tilde{u}_h, v_h) = \sum_{i=1}^{2} \sum_{F \in \mathcal{F}_h^i} \int_{F \cap \Omega^i} \Big(\langle k_i \nabla \tilde{u}_{h,i} \cdot n_F \rangle [\![v_{h,i}]\!] + \langle k_i \nabla v_{h,i} \cdot n_F \rangle [\![\tilde{u}_{h,i}]\!] \Big) \, \mathrm{d}s,$$

$$b_{h,i}(\mu_{h,i}, v_{h,i}) = \sum_{F \in \mathcal{F}_h^i} \frac{k_i h_F}{2} \sum_{N \in \mathcal{N}_F} \mu_{h,i_{|F}}(N) [\![v_{h,i}]\!](N)$$

where $\mathcal{N}_F$ stands for the set of nodes belonging to the edge F. Note that in the definition of $b_{h,i}(\cdot,\cdot)$, the trapezium formula (*i.e.*, the Gauss-Lobatto quadrature formula with 2 points) is used to approximate $\int_F k_i \mu_{h,i} [\![v_{h,i}]\!] \, \mathrm{d}s$.

Lemma 3.4. *The discrete kernel of $b_h(\cdot,\cdot)$ coincides with the space $\mathcal{C}_h$, i.e.,*

$$\mathrm{Ker}\, b_h = \{v_h \in \mathcal{D}_h;\ b_h(\mu_h, v_h) = 0,\ \forall \mu_h \in \mathcal{M}_h\} = \mathcal{C}_h.$$

Proof. Let first $v_h \in \mathcal{C}_h$; the continuity of v_h across any interior edge gives $b_h(\mu_h, v_h) = 0$ for any $\mu_h \in \mathcal{M}_h$, which translates into $v_h \in \mathrm{Ker}\, b_h$. Next, we prove the remaining inclusion, $\mathrm{Ker}\, b_h \subset \mathcal{C}_h$. For $v_h = (v_{h,1}, v_{h,2}) \in \mathrm{Ker}\, b_h$, we consider

$$(\mu_{h,i})_{|F} = h_F^{-1} [\![v_{h,i}]\!], \quad \forall F \in \mathcal{F}_h^i \quad (i = 1, 2).$$

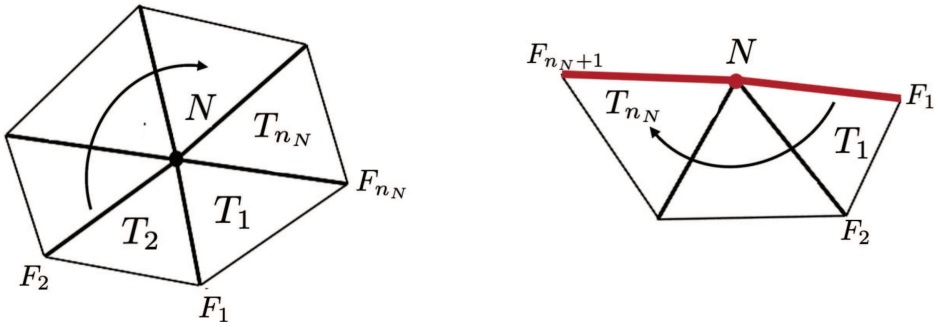

(A) Interior node $N \in \overset{\circ}{\mathcal{N}}{}_h^i$ (B) Boundary node $N \in \mathcal{N}_h^i \setminus \overset{\circ}{\mathcal{N}}{}_h^i$

FIGURE 2. Numbering of triangles and edges on a patch ω_N^i.

Clearly, $\mu_{h,i}$ belongs to $\mathcal{M}_h^i$ since

$$\sum_{F\in\mathcal{F}_N} \mathfrak{s}_N^F h_F(\mu_{h,i})_{|F}(N) = \sum_{F\in\mathcal{F}_N} \mathfrak{s}_N^F [\![v_{h,i}]\!](N) = 0, \quad \forall N \in \overset{\circ}{\mathcal{N}}{}_h^i.$$

From $b_h(\mu_h, v_h) = 0$ we get $[\![v_{h,i}]\!] = 0$ for any $F \in \mathcal{F}_h^i$ $(i = 1, 2)$, which yields $v_h \in \mathcal{C}_h$. The double inclusion yields the announced result. □

We next establish the inf-sup condition for the form $b_h(\cdot,\cdot)$, which holds uniformly with respect to the discretization, the interface, and the diffusion coefficients.

Theorem 3.5. *There exists a constant $\beta > 0$ independent of the mesh size, Γ and K such that*

$$\inf_{\mu_h\in\mathcal{M}_h} \sup_{v_h\in\mathcal{D}_h} \frac{b_h(\mu_h, v_h)}{\|\mu_h\|_{\mathcal{M}_h}\|v_h\|_{\mathcal{D}_h}} \geq \beta.$$

Proof. We follow the idea of [13] for the case of a diffusion problem where the discontinuities of the coefficients are aligned with the mesh, and adapt it here to the CutFEM method. The diffusion coefficients are supposed here to be constant on each subdomain; hence, the analysis provided in [2] for the Laplace operator also applies.

We use Fortin's trick [6]: to any $\mu_h \in \mathcal{M}_h$, we associate a function $v_h \in \mathcal{D}_h$ s.t.

$$b_h(\mu_h, v_h) \gtrsim \|\mu_h\|^2_{\mathcal{M}_h}, \quad \|v_h\|_{\mathcal{D}_h} \lesssim \|\mu_h\|_{\mathcal{M}_h}. \tag{6}$$

Let $\mu_h = (\mu_{h,1}, \mu_{h,2}) \in \mathcal{M}_h$. The construction of $v_h = (v_{h,1}, v_{h,2})$ is done patch-wise. We fix $i \in \{1, 2\}$, consider a node $N \in \mathcal{N}_h^i$ and denote by ω_N^i the patch consisting of the triangles of $\mathcal{T}_h^i$ that share node N. We define $v_{N,i}$ locally on ω_N^i, piecewise linear and discontinuous, by imposing on any edge $F \in \mathcal{F}_h^i \cap \mathcal{F}_N$ that

$$[\![v_{N,i}]\!]_{|F}(N) = h_F(\mu_{h,i})_{|F}(N). \tag{7}$$

We also impose $v_{N,i}(M) = 0$ at all other vertices M of the patch. The linear system (7) is compatible for any $N \in \overset{\circ}{\mathcal{N}}{}_h^i$ due to the constraint imposed in the space $\mathcal{M}_h^i$. In Figure 2 (left), we illustrate the clockwise numbering of the cells and edges on the patch ω_N^i, used to solve system (7). It is also easy to check that the system is compatible when $N \in \mathcal{N}_h^i \setminus \overset{\circ}{\mathcal{N}}{}_h^i$; this case is illustrated in Figure 2 (right).

Then we define $v_{h,i} \in \mathcal{D}_h^i$ as $v_{h,i} = \sum_{N \in \mathcal{N}_h^i} v_{N,i}$, which yields $[\![v_{h,i}]\!]_{|F} = h_F(\mu_{h,i})_{|F}$ for any $F \in \mathcal{F}_h^i$. Hence, we further get that

$$b_h(\mu_h, v_h) = \sum_{i=1}^{2} \sum_{F \in \mathcal{F}_h^i} \frac{k_i h_F^2}{2} \sum_{N \in \mathcal{N}_F} (\mu_{h,i})_{|F}^2(N) \gtrsim \|\mu_h\|_{\mathcal{M}_h}^2 \tag{8}$$

as well as:

$$\sum_{i=1}^{2} \sum_{F \in \mathcal{F}_h^i} \int_F k_i h_F^{-1} [\![v_{h,i}]\!]^2 \, \mathrm{d}s = \sum_{i=1}^{2} \sum_{F \in \mathcal{F}_h^i} \int_F k_i h_F (\mu_{h,i})^2 \, \mathrm{d}s = \|\mu_h\|_{\mathcal{M}_h}^2. \tag{9}$$

It was shown in [13] that (7) admits a solution such that

$$\sum_{T \in \mathcal{T}_h^i} h_T^{-2} \|k_i^{1/2} v_{h,i}\|_T^2 \lesssim \|\mu_{h,i}\|_{\mathcal{M}_h^i}^2 \quad (i = 1, 2). \tag{10}$$

By means of an inverse inequality and using that $\Omega^i \subset \Omega_h^i$, the previous bound implies

$$\sum_{i=1}^{2} \|k_i^{1/2} \nabla v_{h,i}\|_{\Omega^i}^2 \leq \sum_{i=1}^{2} \|k_i^{1/2} \nabla v_{h,i}\|_{\Omega_h^i}^2 \lesssim \|\mu_h\|_{\mathcal{M}_h}^2. \tag{11}$$

In what follows, we bound the remaining terms in the norm $\|v_h\|_{\mathcal{D}_h}$, which are specific to the CutFEM formulation. We clearly have:

$$j_i(v_{h,i}, v_{h,i}) \leq \sum_{F \in \mathcal{F}_g^i} k_i h_F (\|\nabla v_{h,i}^+\|_F^2 + \|\nabla v_{h,i}^-\|_F^2) \lesssim \|k_i^{1/2} \nabla v_{h,i}\|_{\Omega_h^i}^2 \quad (i = 1, 2),$$

so the ghost penalty contribution is uniformly bounded:

$$\sum_{i=1}^{2} j_i(v_{h,i}, v_{h,i}) \lesssim \|\mu_h\|_{\mathcal{M}_h}^2. \tag{12}$$

Thanks to the trace inequality (4), combined with norm equivalence in finite dimensional spaces and with $k_\Gamma \leq k_i$ for $i = 1, 2$, one has for any $T \in \mathcal{T}_h^\Gamma$ that:

$$\int_{\Gamma_T} \frac{k_\Gamma}{h_T} [v_h]^2 \, \mathrm{d}s \lesssim \frac{k_\Gamma}{h_T^2} (\|v_{h,1}\|_T^2 + \|v_{h,2}\|_T^2) \lesssim \frac{1}{h_T^2} (\|k_1^{1/2} v_{h,1}\|_T^2 + \|k_2^{1/2} v_{h,2}\|_T^2).$$

Using again (10), we end up with

$$\sum_{T \in \mathcal{T}_h^\Gamma} \int_{\Gamma_T} \frac{k_\Gamma}{h_T} [v_h]^2 \, \mathrm{d}s \lesssim \|\mu_h\|_{\mathcal{M}_h}^2. \tag{13}$$

Thanks to (8), (9), (11), (12) and (13), we finally obtain (6). □

Lemma 3.4 implies that for any $v_h \in \operatorname{Ker} b_h$,

$$\tilde{a}_h(v_h, v_h) = a_h(v_h, v_h) \gtrsim \|v_h\|_h^2 = \|v_h\|_{\mathcal{D}_h}^2.$$

Hence, we have the uniform coercivity of $\tilde{a}_h(\cdot, \cdot)$ on $\operatorname{Ker} b_h$. Furthermore, the second variational equation of the mixed formulation (5) yields that $\tilde{u}_h$ belongs to $\operatorname{Ker} b_h$, and the well-posedness of the primal formulation (3) ensures that $\tilde{u}_h = u_h$. Finally, the Babuska–Brezzi theorem yields the well-posedness of (5), thanks to Theorem 3.5 which ensures the existence and uniqueness of the multiplier θ_h.

3.3. Local computation of multipliers

A crucial feature of the mixed method is that each multiplier $\theta_{h,i}$ can be computed locally, as sum of local contributions θ_N^i defined on the patches $\omega_N^i = \omega_N \cap \Omega_h^i$ associated to the nodes:

$$\theta_{h,i} = \sum_{N \in \mathcal{N}_h^i} \theta_N^i, \qquad i = 1, 2. \tag{14}$$

Next, we present the local computation on each subdomain Ω_h^i $(i = 1, 2)$.

For this purpose, let the residual $r_h(\cdot) := l_h(\cdot) - \tilde{a}_h(u_h, \cdot)$. For convenience of notation, we also introduce for any $v_{h,i} \in \mathcal{D}_h^i$:

$$r_{h,1}(v_{h,1}) = r_h((v_{h,1}, 0)), \quad r_{h,2}(v_{h,2}) = r_h((0, v_{h,2})).$$

From (5), we immediately have that

$$b_{h,i}(\theta_{h,i}, v_{h,i}) = r_{h,i}(v_{h,i}) \quad \forall v_{h,i} \in \mathcal{D}_h^i \quad (i = 1, 2), \tag{15}$$

whereas from Lemma 3.4, we obtain that $r_{h,i}(v_{h,i}) = 0$ for any $v_{h,i} \in \mathcal{C}_h^i$ and $i = 1, 2$.

Let now $i \in \{1, 2\}$ and $N \in \mathcal{N}_h^i$. We define $\theta_N^i \in \mathcal{M}_h^i$ living on $\mathcal{F}_N^i := \mathcal{F}_N \cap \mathcal{F}_h^i$ such that, for any triangle $T \in \omega_N^i$:

$$b_{h,i}(\theta_N^i, \varphi_N \chi_T) = r_{h,i}(\varphi_N \chi_T), \tag{16}$$

$$b_{h,i}(\theta_N^i, \varphi_M \chi_T) = 0, \qquad \forall M \in \mathcal{N}_T \setminus \{N\} \tag{17}$$

where φ_N, φ_M are the P^1-nodal basis functions associated to the nodes N and M, respectively, χ_T is the characteristic function on T, and $\mathcal{N}_T$ is the set of nodes in T. Note that (17) implies that $\theta_N^i(M) = 0$ for all $M \in \mathcal{N}_T \setminus \{N\}$ and $T \in \omega_N^i$.

Using a similar technique as in [2], one can show that θ_N^i is well-defined, thanks to the constraint imposed in the space $\mathcal{M}_h^i$, and that $\tilde{\theta}_{h,i} := \sum_{N \in \mathcal{N}_h^i} \theta_N^i$ satisfies the weak equation (15). Hence, $\tilde{\theta}_h = (\tilde{\theta}_{h,1}, \tilde{\theta}_{h,2})$ belongs to $\mathcal{M}_h$ and satisfies the mixed problem (5), so by uniqueness of its solution we get $\tilde{\theta}_h = \theta_h$ and (14) is checked.

Moreover, similarly to [13] we get that:

$$\left(\sum_{F \in \mathcal{F}_N \cap \mathcal{F}_h^i} h_F k_i^2 \|\theta_N^i\|_F^2 \right)^{1/2} \lesssim \sum_{T \in \omega_N^i} |r_{h,i}(\varphi_N \chi_T)|. \tag{18}$$

In the sequel, we bound θ_N^i in terms of the solution u_h and the data; this estimate is useful in the *a posteriori* error analysis.

Theorem 3.6. *For $i \in \{1, 2\}$ and $N \in \mathcal{N}_h^i$, we have that:*

$$\begin{aligned} \left(\sum_{F \in \mathcal{F}_N \cap \mathcal{F}_h^i} h_F k_i^2 \|\theta_N^i\|_F^2 \right)^{1/2} \lesssim & \sum_{T \in \omega_N^i} \sqrt{h_T} k_i \left(\|[\![\partial_n u_{h,i}]\!]\|_{\partial T \setminus \partial \omega_N^i} + \|[\![\partial_n u_{h,i}]\!]\|_{\partial T \cap \mathcal{F}_g^i} \right) \\ & + \sum_{T \in \mathcal{T}_h^\Gamma \cap \omega_N^i} \left(\frac{k_\Gamma}{\sqrt{h_T}} \|[u_h]\|_{\Gamma_T} + \sqrt{h_T} \|g - [K \nabla u_h \cdot n_\Gamma]\|_{\Gamma_T} \right) + \sum_{T \in \omega_N^i} h_T \|f\|_{T^i}. \end{aligned}$$

Proof. Thanks to inequality (18), we only need to bound the residual $r_{h,i}(\varphi_N\chi_T)$. In the following, without loss of generality, we prove the bound for $i=1$. For any $T\in\omega_N^1$, we have that:

$$\begin{aligned} r_{h,1}(\varphi_N\chi_T) = &\int_{T^1} f\varphi_N\,\mathrm{d}x + \int_{\Gamma_T} g\omega_2\varphi_N\,\mathrm{d}s - \int_{T^1} k_1\nabla u_{h,1}\cdot\nabla\varphi_N\,\mathrm{d}x \\ &- \gamma h_T^{-1}\int_{\Gamma_T} k_\Gamma[u_h]\varphi_N\,\mathrm{d}s + \int_{\Gamma_T}(\{K\nabla u_h\cdot n_\Gamma\}\varphi_N + \omega_1 k_1\nabla\varphi_N\cdot n_\Gamma[u_h])\,\mathrm{d}s \\ &+ \sum_{F\in\mathcal{F}_T\cap\mathcal{F}_h^1}\int_{F\cap\Omega^1}\langle k_1\nabla u_{h,1}\cdot n_F\rangle[\![\varphi_N\chi_T]\!]\,\mathrm{d}s - \sum_{F\in\mathcal{F}_T\cap\mathcal{F}_g^1}\gamma_g h_F\int_F [\![k_1\nabla u_{h,1}\cdot n_F]\!][\![\nabla(\varphi_N\chi_T)\cdot n_F]\!]\,\mathrm{d}s, \end{aligned}$$

where $\mathcal{F}_T$ denotes the set of sides of the triangle T. Here above, we have used that $[\varphi_N\chi_T]_{|\Gamma_T} = (\varphi_N)_{|\Gamma_T}$ since n_Γ points from Ω^1 to Ω^2. Using integration by parts for the third term on the right-hand side further yields:

$$\begin{aligned} r_{h,1}(\varphi_N\chi_T) = &\int_{T^1} f\varphi_N dx + \omega_2\int_{\Gamma_T}(g-[K\nabla u_h\cdot n_\Gamma])\varphi_N ds + \omega_1\int_{\Gamma_T} k_1\nabla\varphi_N\cdot n_\Gamma[u_h]ds \\ &- \gamma h_T^{-1}\int_{\Gamma_T} k_\Gamma[u_h]\varphi_N\,\mathrm{d}s - \frac{1}{2}\int_{\partial T^1\setminus\Gamma_T} k_1[\![\partial_n u_{h,1}]\!]\varphi_N\,\mathrm{d}s \\ &- \sum_{F\in\mathcal{F}_T\cap\mathcal{F}_g^1}\gamma_g h_F\int_F k_1[\![\partial_n u_{h,1}]\!][\![\nabla(\varphi_N\chi_T)\cdot n_F]\!]\,\mathrm{d}s. \end{aligned}$$

If T is not a cut element, then the integrals over Γ_T vanish. By the Cauchy–Schwarz inequality and using $\omega_1 k_1 = k_\Gamma$ and $\varphi_N = 0$ on $\partial\omega_N^1$, we next get:

$$\begin{aligned} |r_{h,1}(\varphi_N\chi_T)| \lesssim\ &\|f\|_{T^1}\|\varphi_N\|_{T^1} + \omega_2\|g-[K\nabla u_h\cdot n_\Gamma]\|_{\Gamma_T}\|\varphi_N\|_{\Gamma_T} \\ &+ k_\Gamma\|[u_h]\|_{\Gamma_T}(\|\nabla\varphi_N\|_{\Gamma_T} + \gamma h_T^{-1}\|\varphi_N\|_{\Gamma_T}) \\ &+ \gamma_g h_F k_1\|[\![\partial_n u_{h,1}]\!]\|_{\partial T\cap\mathcal{F}_g^1}\|\nabla\varphi_N\|_{\partial T} + k_1\|[\![\partial_n u_{h,1}]\!]\|_{\partial T\setminus\partial\omega_N^1}\|\varphi_N\|_{\partial T}. \end{aligned}$$

Using the following bounds for the nodal basis function φ_N:

$$\begin{aligned} &\|\varphi_N\|_{T^1}\le\|\varphi_N\|_T\lesssim h_T,\quad \|\varphi_N\|_{\partial T}\lesssim\sqrt{h_T}, \\ &\|\nabla\varphi_N\|_{\partial T}\lesssim\frac{1}{\sqrt{h_T}},\quad \|\varphi_N\|_{\Gamma_T}\lesssim\frac{1}{\sqrt{h_T}}\|\varphi_N\|_T\lesssim\sqrt{h_T}, \end{aligned}$$

one finally gets, with $\omega_2\le 1$, that:

$$\begin{aligned} |r_{h,1}(\varphi_N\chi_T)| \lesssim\ &h_T\|f\|_{T^1} + h_T^{1/2}\|g-[K\nabla u_h\cdot n_\Gamma]\|_{\Gamma_T} + k_\Gamma h_T^{-1/2}\|[u_h]\|_{\Gamma_T} \\ &+ k_1 h_T^{1/2}(\|[\![\partial_n u_{h,1}]\!]\|_{\partial T\cap\mathcal{F}_g^1} + \|[\![\partial_n u_{h,1}]\!]\|_{\partial T\setminus\partial\omega_N^1}). \end{aligned} \tag{19}$$

The terms on Γ_T on the right-hand side of (19) vanish when $T\in\mathcal{T}_h\setminus\mathcal{T}_h^\Gamma$. This ends the theorem's proof. □

Remark 3.7. The previous approach can be extended to an arbitrary polynomial degree $m\in\mathbb{N}^*$, following [13]. More precisely, if the discrete solution $u_{h,i}$ is piecewise P^m (with suitable ghost-penalty stabilization), then a well-posed mixed formulation can still be derived and $\theta_{h,i}$ can still be computed locally, with $\theta_{h,i}\in P^m(F)$ on any edge F. The proofs combine the arguments of [13] for arbitrary polynomial degree m on fitted meshes with the preceding ones addressing the treatment of unfitted meshes.

4. Local flux reconstruction

In this section, we propose a reconstruction of a discrete, element-wise conservative flux σ_h, approximation of the continuous flux $\sigma := K\nabla u$, based on the CutFEM solution u_h and the multiplier θ_h. An innovative feature is the use of an immersed Raviart–Thomas space (cf. [22]) on the cut elements, which leads to a reliable and locally efficient flux-based *a posteriori* error estimator.

The use of the classical Raviart–Thomas space $\mathcal{RT}^0(\mathcal{T}_h)$, while yielding a conservative flux in $H(\mathrm{div},\Omega)$ and admitting a natural extension to higher polynomial degrees, does not in general yield a locally efficient flux-based estimator on cut elements. We refer to [20], page 120 and the subsequent discussion, for further details. For this reason, one is led to employ piecewise or immersed Raviart–Thomas-type spaces on cut elements.

In order to simplify the presentation, we assume in the sequel, without loss of generality, that no edge $F \in \mathcal{F}_h$ is situated entirely on Γ.

4.1. The immersed Raviart–Thomas space $\mathcal{IRT}^0(\mathcal{T}_h)$

We begin by recalling the definition of the lowest-order immersed Raviart–Thomas space, recently introduced in [22]. On a non-cut element $T \in \mathcal{T}_h\backslash\mathcal{T}_h^\Gamma$, the polynomial space is the standard Raviart–Thomas space of lowest degree $\mathcal{RT}^0(T)$. We recall that

$$\mathcal{RT}^0(\mathbb{R}^2) = \left\{ \phi \in P^1(\mathbb{R}^2)^2;\ \phi(x_1,x_2) = \begin{pmatrix} a \\ b \end{pmatrix} + c \begin{pmatrix} x_1 \\ x_2 \end{pmatrix},\ a,\ b,\ c \in \mathbb{R} \right\}$$

and that for $\omega \subset \mathbb{R}^2$, we set $\mathcal{RT}^0(\omega) = \{\psi_{|\omega};\ \psi \in \mathcal{RT}^0(\mathbb{R}^2)\}$.

In order to introduce the new finite element space on a cut cell $T \in \mathcal{T}_h^\Gamma$, let t_Γ denote the unit tangent vector to Γ, oriented by a 90° clockwise rotation of n_Γ, and recall that $T^i = T \cap \Omega^i$ $(i = 1,2)$. The local immersed Raviart–Thomas space $\mathcal{IRT}^0(T)$ is defined in [22] as the set of piecewise $\mathcal{RT}^0$-functions ψ, such that $\psi_i := \psi_{|T^i}$ belong to $\mathcal{RT}^0(T)$ for $i = 1,2$ and satisfy the following conditions:

$$\begin{cases} [\psi \cdot n_\Gamma] = \psi_1 \cdot n_\Gamma - \psi_2 \cdot n_\Gamma = 0, \\ [K^{-1}\psi \cdot t_\Gamma](x_\Gamma) = k_1^{-1}\psi_1 \cdot t_\Gamma(x_\Gamma) - k_2^{-1}\psi_2 \cdot t_\Gamma(x_\Gamma) = 0, \\ \mathrm{div}\,\psi_1 = \mathrm{div}\,\psi_2. \end{cases} \tag{20}$$

Here above, x_Γ is an arbitrary point of Γ_T. We recall that for $i = 1,2$, $(\psi_i \cdot n_\Gamma)_{|\Gamma_T}$ and $(\mathrm{div}\,\psi_i)_{|T}$ are constant, whereas $(\psi_i \cdot t_\Gamma)_{|\Gamma_T}$ is *a priori* linear.

The condition $[\psi \cdot n_\Gamma] = 0$ ensures that $\mathcal{IRT}^0(T) \subset H(\mathrm{div},T)$ and that the (homogeneous) transmission condition across the interface is strongly satisfied. Meanwhile, the other condition on Γ, $[K^{-1}\psi \cdot t_\Gamma](x_\Gamma) = 0$ takes into account the fact that $[\nabla u \cdot t_\Gamma](x_\Gamma) = 0$, since $[u] = 0$. Finally, the last condition of (20) ensures that $\dim \mathcal{IRT}^0(T) = \dim \mathcal{RT}^0(T) = 3$.

On each element $T \in \mathcal{T}_h$, the local degrees of freedom are the same as for the standard $\mathcal{RT}^0$ space, that is:

$$N_{T,j}(\psi) = \frac{1}{|F_j|}\int_{F_j} \psi \cdot n_T \,\mathrm{d}s, \quad 1 \le j \le 3, \tag{21}$$

where $(F_j)_{1\le j\le 3}$ denote the edges of T. The global space $\mathcal{IRT}^0(\mathcal{T}_h)$ is then defined as the set of functions ψ such that for any $T \in \mathcal{T}_h\backslash\mathcal{T}_h^\Gamma$, $\psi_{|T} \in \mathcal{RT}^0(T)$, whereas for any $T \in \mathcal{T}_h^\Gamma$, $\psi_{|T} \in \mathcal{IRT}^0(T)$. In addition, we impose continuity of the shared degrees of freedom, which means that ψ satisfies the following property:

$$\int_F [\![\psi \cdot n_F]\!]\,\mathrm{d}s := \sum_{i=1}^{2} \int_{F^i} [\![\psi_i \cdot n_F]\!]\,\mathrm{d}s = 0, \quad \forall F \in \mathcal{F}_h^{int}.$$

Note that contrarily to the $\mathcal{RT}^0(\mathcal{T}_h)$ space, for a function $\psi \in \mathcal{IRT}^0(T)$ and a cut edge $F \in \mathcal{F}_h^\Gamma$, $(\psi \cdot n_F)_{|F}$ is only piecewise constant on the edge F. Thus, condition $\int_F [\![\psi \cdot n_F]\!]\,\mathrm{d}s = 0$ does not imply $[\![\psi \cdot n_F]\!]_{|F} = 0$. Hence, $\mathcal{IRT}^0(\mathcal{T}_h) \not\subset H(\mathrm{div},\Omega)$.

Remark 4.1. To the best of our knowledge, only the lowest-order immersed Raviart–Thomas $\mathcal{IRT}^0(\mathcal{T}_h)$ space has been fully developed in the literature; the extension to higher-order immersed spaces remains an active area of research. Possible definitions of the immersed Raviart–Thomas space $\mathcal{IRT}^1(\mathcal{T}_h)$, together with the associated flux, are discussed in [20], p. 170. More precisely, on a cut triangle T, the local space $\mathcal{IRT}^1(T)$ is defined analogously to $\mathcal{IRT}^0(T)$, as the set of piecewise $\mathcal{RT}^1$-functions ψ satisfying conditions (20). Note that, for $i \in \{1,2\}$, both $\psi_i \cdot n_\Gamma$ and $\operatorname{div} \psi_i$ are now P^1 polynomials; hence, the equations $[\psi \cdot n_\Gamma] = 0$ and $\operatorname{div} \psi_1 = \operatorname{div} \psi_2$ yield two and three scalar constraints, respectively. In order to ensure that $\dim \mathcal{IRT}^1(T) = \dim \mathcal{RT}^1(T) = 8$, two additional scalar constraints are required. One possible choice is to impose

$$\int_{T^\triangle} \psi_1 \, \mathrm{d}x = \int_{T^\triangle} \psi_2 \, \mathrm{d}x,$$

where $T^\triangle$ denotes the triangular subregion (T^1 or T^2) obtained by cutting T with Γ (see Fig. 3 for an illustration). The preliminary results reported in [20] suggest that $\mathcal{IRT}^1(T)$ satisfies the unisolvency property. Its degrees of freedom coincide with those of the standard $\mathcal{RT}^1$ space. The global space $\mathcal{IRT}^1(\mathcal{T}_h)$ is obtained by imposing weak continuity of the normal traces:

$$\int_F [\![\psi \cdot n_F]\!] \, p \, \mathrm{d}s = 0, \quad \forall F \in \mathcal{F}_h^{int}, \, \forall p \in P^1(F).$$

Next, we build an element-wise conservative flux in the $\mathcal{IRT}^0(\mathcal{T}_h)$ space. We consider the transmission condition $[\sigma \cdot n_\Gamma] = g$ on Γ in both the homogeneous and the non-homogeneous cases.

4.2. Homogeneous Neumann transmission condition

We assume here that $g = 0$ and reconstruct a flux σ_h in the space $\mathcal{IRT}^0(\mathcal{T}_h)$. This flux will then strongly satisfy the transmission condition across the interface, thanks to the definition of the immersed Raviart–Thomas space. We define σ_h by imposing its degrees of freedom as follows:

– for any $F \in \mathcal{F}_h^i \backslash \mathcal{F}_h^\Gamma$ $(i = 1, 2)$, we set

$$\int_F \sigma_h \cdot n_F \, \mathrm{d}s = \int_F \langle k_i \nabla u_{h,i} \cdot n_F \rangle \, \mathrm{d}s - \int_F k_i \theta_{h,i} \, \mathrm{d}s \tag{22}$$

– for any cut edge $F \in \mathcal{F}_h^\Gamma$, we set

$$\int_F \sigma_h \cdot n_F \, \mathrm{d}s = \sum_{i=1}^{2} \left(\int_{F^i} \langle k_i \nabla u_{h,i} \cdot n_F \rangle \, \mathrm{d}s - \int_F k_i \theta_{h,i} \, \mathrm{d}s \right). \tag{23}$$

We can equivalently write the equations (22) and (23) as follows:

$$\begin{aligned} \sigma_h \cdot n_F &= \langle k_i \nabla u_{h,i} \cdot n_F \rangle - k_i \pi_F^0 \theta_{h,i}, && \forall F \in \mathcal{F}_h^i \backslash \mathcal{F}_h^\Gamma \quad (i = 1, 2), \\ \int_F \sigma_h \cdot n_F \, \mathrm{d}s &= \sum_{i=1}^{2} \left(\int_{F^i} \langle k_i \nabla u_{h,i} \cdot n_F \rangle \, \mathrm{d}s - k_i h_F \pi_F^0 \theta_{h,i} \right), && \forall F \in \mathcal{F}_h^\Gamma. \end{aligned}$$

Note that $\sigma_h \cdot n_F$ is only piecewise constant on the cut edges, but it belongs to $H(\operatorname{div}, T)$ for any cut triangle $T \in \mathcal{T}_h^\Gamma$. Next, we establish the element-wise conservation property.

Theorem 4.2. *One has that*

$$-(\operatorname{div} \sigma_h)_{|T} = \pi_T^0 f, \quad \forall T \in \mathcal{T}_h. \tag{24}$$

Proof. Let $T \in \mathcal{T}_h$. We start from $\int_T \operatorname{div} \sigma_h \, \mathrm{d}x = \int_{\partial T} \sigma_h \cdot n_T \, \mathrm{d}s$ and use the flux definition (22) and (23). On a non-cut cell, we obtain (24) by testing the mixed formulation (5) with $(\chi_T, 0)$ if $T \in \mathcal{T}_h^1$, and with $(0, \chi_T)$ if $T \in \mathcal{T}_h^2$.

So in the sequel, we focus on a cut cell $T \in \mathcal{T}_h^\Gamma$ and test (5) with $v_h = (\chi_T, \chi_T)$. This yields that on any cell $T' \in \mathcal{T}_h$ one has that $(\nabla v_{h,i})_{|T'} = 0$, hence

$$a_i(u_{h,i}, v_{h,i}) = j_i(u_{h,i}, v_{h,i}) = 0, \quad i = 1, 2. \tag{25}$$

Moreover, one also has that

$$a_\Gamma(u_h, v_h) = \sum_{T' \in \mathcal{T}_h^\Gamma} \int_{\Gamma_{T'}} \left(\frac{\gamma k_\Gamma}{h_{T'}} [u_h] - \{K \nabla u_h \cdot n_\Gamma\} \right) [v_h] \, \mathrm{d}s = 0, \tag{26}$$

since for any cut cell $T' \in \mathcal{T}_h^\Gamma$, one has $(v_{h,1})_{|T'} = (v_{h,2})_{|T'}$ and therefore, $[v_h]_{|\Gamma_{T'}} = 0$.

Next, for any $F \subset \partial T$, we can write that

$$\sigma_h \cdot n_T|_F = \sigma_h \cdot n_F [\![v_h]\!],$$

so we obtain, using (22) and (23), as well as $b_{h,i}(\theta_h, v_h) = \sum_{F \in \mathcal{F}_T} \int_F k_i \theta_{h,i} \, \mathrm{d}s$, that

$$-\int_T \operatorname{div} \sigma_h \, \mathrm{d}x = -\sum_{F \in \mathcal{F}_T} \int_F \sigma_h \cdot n_F [\![v_h]\!] \, \mathrm{d}s = -d_h(u_h, v_h) + b_h(\theta_h, v_h).$$

Using next the definition of $\tilde{a}_h(\cdot, \cdot)$, as well as (25) and (26), we further get:

$$-\int_T \operatorname{div} \sigma_h \, \mathrm{d}x = \tilde{a}_h(u_h, v_h) + b_h(\theta_h, v_h) = l_h(v_h) = \int_T f \, \mathrm{d}x,$$

which yields the desired relation (24). □

Note that the definition of the flux remains unchanged if one imposes $[u] = \chi$ on Γ in the model problem (1). The only required modifications consist in replacing $[u_h]$ by $[u_h] - \chi$ in the estimate of Theorem 3.6 and in relation (26), without affecting the statement of Theorem 4.2.

Remark 4.3. One can also define (see [20]) a flux $\sigma_h \in \mathcal{IRT}^1(\mathcal{T}_h)$ by imposing its degrees of freedom, similarly to (22) and (23):

– for $F \in \mathcal{F}_h^i \backslash \mathcal{F}_h^\Gamma$ $(i = 1, 2)$,

$$\int_F \sigma_h \cdot n_F \varphi \, \mathrm{d}s = \int_F \langle k_i \nabla u_{h,i} \cdot n_F \rangle \, \varphi \, \mathrm{d}s - \int_F k_i \theta_{h,i} \varphi \, \mathrm{d}s, \quad \forall \varphi \in P^1(F);$$

– for $F \in \mathcal{F}_h^\Gamma$,

$$\int_F \sigma_h \cdot n_F \varphi \, \mathrm{d}s = \sum_{i=1}^2 \left(\int_{F^i} \langle k_i \nabla u_{h,i} \cdot n_F \rangle \, \varphi \, \mathrm{d}s - \int_F k_i \theta_{h,i} \varphi \, \mathrm{d}s \right), \quad \forall \varphi \in P^1(F);$$

– for $T \in \mathcal{T}_h$,

$$\begin{aligned} \int_T \sigma_h \cdot \zeta \, \mathrm{d}x = & \sum_{i=1}^2 \int_{T^i} k_i \nabla u_{h,i} \cdot \zeta \, \mathrm{d}x - \int_{\Gamma_T} \{k \zeta \cdot n_\Gamma\} \, [u_h] \, \mathrm{d}s \\ & + \sum_{i=1}^2 \sum_{F \in \mathcal{F}_g^i \cap \mathcal{F}_T} \gamma_g h_F \int_F k_i \, [\![\nabla u_{h,i} \cdot n_F]\!] \, [\![\zeta \cdot n_F]\!] \, \mathrm{d}s, \quad \forall \zeta \in \left(P^0(T) \right)^2. \end{aligned}$$

Then one can prove, similarly to Theorem 4.2, that $(\operatorname{div} \sigma_h)_{|T} = -\pi_T^1 f$, for any $T \in \mathcal{T}_h$.

4.3. Non-homogeneous Neumann transmission condition

We can now treat the general case $g \neq 0$. For any $T \in \mathcal{T}_h^\Gamma$, we set $g_h = \pi^0_{\Gamma_T} g$ and define the linear continuous operator $\mathcal{L}_T : \mathcal{RT}^0(T^1) \times \mathcal{RT}^0(T^2) \longrightarrow \mathbb{R}^6$ such that for any $\tau = (\tau_1, \tau_2)$,

$$\mathcal{L}_T(\tau_1, \tau_2) = \left(\left(\int_{F_j} \tau \cdot n_{F_j} \, \mathrm{d}s \right)_{1 \leq j \leq 3}, [\tau \cdot n_\Gamma], \operatorname{div} \tau_1 - \operatorname{div} \tau_2, [K^{-1}\tau \cdot t_\Gamma](x_T) \right),$$

where on a cut side F, we have that

$$\int_F \tau \cdot n_F \, \mathrm{d}s = \sum_{i=1}^{2} \int_{F^i} \tau_i \cdot n_F \, \mathrm{d}s.$$

The operator $\mathcal{L}_T$ is injective due to the unisolvency of the $\mathcal{IRT}^0(T)$ space, and therefore surjective. Hence, there exists a unique flux

$$\sigma_T^g = (\sigma_1^g, \sigma_2^g) \in \mathcal{RT}^0(T^1) \times \mathcal{RT}^0(T^2)$$

such that $\mathcal{L}_T(\sigma_T^g) = (0, 0, 0, g_h, 0, 0)$. We denote by σ^g the zero extension to Ω: $\sigma^g = \sum_{T \in \mathcal{T}_h^\Gamma} \sigma_T^g \chi_T$. We now define the global flux σ_h^g as follows:

$$\sigma_h^g = \sigma_h + \sigma^g, \tag{27}$$

where $\sigma_h \in \mathcal{IRT}^0(\mathcal{T}_h)$ is the flux corresponding to $g = 0$, defined by (22) and (23).

We can establish the following conservation property. On a cut triangle T, we use the discrete divergence operator div_h defined, for a function τ such that $\tau_{|T^i} \in H(\operatorname{div}, T^i)$, by $(\operatorname{div}_h \tau)_{|T^i} = \operatorname{div}(\tau_{|T^i})$ for $i = 1, 2$.

Theorem 4.4. *One has that*

$$-(\operatorname{div}_h \sigma_h^g)_{|T} = \pi_T^0 f, \quad \forall T \in \mathcal{T}_h. \tag{28}$$

Proof. We treat here only the case of a cut cell $T \in \mathcal{T}_h^\Gamma$. As in the proof of Theorem 4.2, we have:

$$-\int_T \operatorname{div} \sigma_h \, \mathrm{d}x = l_h(v_h) = \int_T f \, \mathrm{d}x + \int_{\Gamma_T} g \, \mathrm{d}s. \tag{29}$$

Note that we also have, integrating by parts on each T^i and using the degrees of freedom of σ^g, that:

$$\int_T \operatorname{div}_h \sigma^g \, \mathrm{d}x = \sum_{i=1}^{2} \int_{T^i} \operatorname{div} \sigma_i^g \, \mathrm{d}x = \int_{\Gamma_T} [\sigma^g \cdot n_\Gamma] \, \mathrm{d}s = \int_{\Gamma_T} g_h \, \mathrm{d}s. \tag{30}$$

Using (29), (30) and the definition (27), we immediately obtain:

$$\int_T \operatorname{div}_h \sigma_h^g \, \mathrm{d}x = \int_T \operatorname{div} \sigma_h \, \mathrm{d}x + \int_T \operatorname{div}_h \sigma^g \, \mathrm{d}x = -\int_T f \, \mathrm{d}x,$$

and, hence, the announced result. □

5. Application to *a posteriori* error analysis

For the sake of simplicity, we assume here that $g = 0$ although the analysis also applies to the case $g \neq 0$.

We set $\tau_h = K^{-1/2}(\sigma_h - K\nabla_h u_h)$, where $\sigma_h \in \mathcal{IRT}^0(\mathcal{T}_h)$ is the flux introduced in Subsection 4.2, and we define the *a posteriori* local error estimator:

$$\eta_T = \|K^{-1/2}(\sigma_h - K\nabla_h u_h)\|_T = \|\tau_h\|_T, \quad \forall T \in \mathcal{T}_h.$$

Since u_h is discontinuous across Γ, we use the discrete gradient ∇_h in a cut triangle $T \in \mathcal{T}_h^\Gamma$; thus, $\nabla_h u_h \in L^2(T)$ is defined by its L^2-restriction to each subdomain:

$$(\nabla_h u_h)_{|T\cap\Omega^i} = (\nabla u_{h,i})_{|T\cap\Omega^i}, \quad 1 \le i \le 2.$$

In addition, on the cut cells $T \in \mathcal{T}_h^\Gamma$ we also consider

$$\tilde{\eta}_T = \frac{\sqrt{h_T k_\Gamma}}{\sqrt{h_T^{\min}|\Gamma_T|}} \|[u_h]\|_{\Gamma_T}, \quad \forall T \in \mathcal{T}_h^\Gamma,$$

where $h_T^{\min} = \min\{|F^i|;\ F \in \partial T \cap \mathcal{F}_h^\Gamma,\ 1 \le i \le 2\}$.

We introduce another local estimator on the cut edges:

$$\eta_F = \frac{\sqrt{h_F}}{\sqrt{k_\Gamma}} \|[\![\sigma_h \cdot n_F]\!] - \pi_F^0 [\![\sigma_h \cdot n_F]\!]\|_F = \frac{\sqrt{h_F}}{\sqrt{k_\Gamma}} \|[\![\sigma_h \cdot n_F]\!]\|_F, \quad \forall F \in \mathcal{F}_h^\Gamma.$$

The corresponding global error estimators are given by:

$$\eta = \left(\sum_{T\in\mathcal{T}_h} \eta_T^2 \right)^{1/2}, \qquad \eta_\Gamma = \left(\sum_{F\in\mathcal{F}_h^\Gamma} \eta_F^2 + \sum_{T\in\mathcal{T}_h^\Gamma} \tilde{\eta}_T^2 \right)^{1/2},$$

while the data approximation term is given by

$$\epsilon(\Omega) = \left(\sum_{T\in\mathcal{T}_h} \frac{h_T^2}{\delta_T} \|f - \pi_T^0 f\|_T^2 \right)^{1/2}, \qquad \delta_T = \begin{cases} k_i & \text{if } T \in \mathcal{T}_h^i \backslash \mathcal{T}_h^\Gamma, \\ k_\Gamma & \text{if } T \in \mathcal{T}_h^\Gamma. \end{cases}$$

We similarly define $\epsilon(\omega)$ for a set $\omega \subset \mathbb{R}^2$ which is a union of cells.

Remark 5.1. The treatment of the non-homogeneous jump condition $[u] = \chi$ on Γ requires a modification of $\tilde{\eta}_T$. More precisely, the term $[u_h]$ is replaced by $[u_h] - \chi_h$, where χ_h denotes the continuous, piecewise linear approximation of χ, assumed to belong to $C^0(\Gamma)$. In addition, an extra higher-order term must be incorporated into $\epsilon(\Omega)$ to account for the approximation of the data χ by χ_h.

Remark 5.2. The non-homogeneous Neumann condition $[K\nabla u \cdot n_\Gamma] = g$ on Γ can be treated in a similar manner, by adding a further higher-order term to $\epsilon(\Omega)^2$, namely $\sum_{T\in\mathcal{T}_h^\Gamma} \frac{h_T}{k_\Gamma} \|g - g_h\|_{\Gamma_T}^2$. With this modification, all the proofs presented in [11] for the case $g = 0$ remain valid for $g \neq 0$, by replacing $\|[K\nabla u_h \cdot n_\Gamma]\|_{\Gamma_T}$ with $\|g_h - [K\nabla u_h \cdot n_\Gamma]\|_{\Gamma_T}$.

We have established in [11] the following error bounds regarding the reliability and local efficiency of the *a posteriori* estimator $\eta + \eta_\Gamma$.

Theorem 5.3 (Reliability)**.** *Let u and u_h be the solutions of (2) and (3), respectively. There exists a constant $C > 0$ independent of the mesh, the coefficients and the interface such that*

$$\left(\sum_{i=1}^{2} \|k_i^{1/2} \nabla(u - u_{h,i})\|_{\Omega^i}^2 \right)^{1/2} \le \eta + C\left(\eta_\Gamma + \epsilon(\Omega)\right). \tag{31}$$

The previous theorem shows that the weighted H^1 semi-norm of the error is bounded by the main estimator η with a reliability constant equal to 1, in agreement with well-known results for equilibrated flux-based estimators. The additional estimator η_Γ and the higher-order term $\epsilon(\Omega)$ in estimate (31) are multiplied by a constant which

is independent of the mesh size, the diffusion coefficients and the interface geometry, and depends only on the shape regularity of the mesh.

Note that one can also control the two remaining contributions to the energy norm of the error, namely the Nitsche stabilisation on Γ and the ghost-penalty stabilisation. Indeed, the first one is immediately bounded by η_Γ, using the facts that $h_T^{\min} \leq h_T$ and $|\Gamma_T| \leq h_T$ for any cut triangle T:

$$\left(\sum_{T\in\mathcal{T}_h^\Gamma} \frac{k_\Gamma}{h_T}\|[u_h]\|_{\Gamma_T}^2\right)^{1/2} \leq \left(\sum_{T\in\mathcal{T}_h^\Gamma} \tilde{\eta}_T^2\right)^{1/2} \leq \eta_\Gamma.$$

The bound for the second term, $(\sum_{i=1}^2 j_i(u_{h,i},u_{h,i}))^{1/2}$, is more technical and is detailed in the next lemma.

Lemma 5.4. *Let* $C_h^\Gamma := \max_{T\in\mathcal{T}_h^\Gamma} \frac{\sqrt{h_T}}{\sqrt{h_T^{\min}}}$. *Then one has that*

$$\left(\sum_{i=1}^2 j_i(u_{h,i},u_{h,i})\right)^{1/2} \lesssim C_h^\Gamma \frac{k_{\max}^{1/2}}{k_{\min}^{1/2}} \left(\eta + \eta_\Gamma + \epsilon(\Omega)\right).$$

Proof. We recall that $j_i(u_{h,i},u_{h,i}) = \sum_{F\in\mathcal{F}_g^i} h_F k_i \|[\![\partial_n u_{h,i}]\!]\|_F^2$. For $i\in\{1,2\}$ and $F\in\mathcal{F}_g^i$, using the facts that $[\![\partial_n u_{h,i}]\!]$ is constant on F and $[\![\partial_n u]\!] = 0$ on $F^i = F\cap\Omega^i$, we have

$$\|[\![\partial_n u_{h,i}]\!]\|_F^2 = \frac{h_F}{|F^i|}\|[\![\partial_n u_{h,i}]\!]\|_{F^i}^2 \leq 2\frac{h_F}{|F^i|}\|[\![\partial_n(u_{h,i}-I_h u_h)]\!]\|_{F^i}^2 + 2\frac{h_F}{h_F^{\min}}\|[\![\partial_n(I_h u_h - u)]\!]\|_{F^i}^2, \tag{32}$$

where $I_h u_h \in H^1(\Omega)$ is the interpolation of u_h introduced in [11], which coincides with u_h on the non-cut triangles. If the ghost edge F is cut, then it belongs to both $\mathcal{F}_g^1$ and $\mathcal{F}_g^2$, and the last right-hand side term of (32) is summed over the index i; thus, it yields the norm on the whole edge F:

$$\sum_{i=1}^2 h_F k_i \|[\![\partial_n(u-I_h u_h)]\!]\|_{F^i}^2 \leq h_F k_{\max}\|[\![\partial_n(u-I_h u_h)]\!]\|_F^2,$$

which can be further bounded using the classical Verfürth argument based on cut-off functions:

$$h_F\|[\![\partial_n(u-I_h u_h)]\!]\|_F^2 \lesssim |u-I_h u_h|_{1,T_F^+\cup T_F^-}^2 + \frac{1}{k_{\min}}\epsilon(T_F^+\cup T_F^-)^2.$$

Using also the triangle inequality, we finally obtain on a cut ghost edge F that:

$$\sum_{i=1}^2 h_F k_i \|[\![\partial_n(u-I_h u_h)]\!]\|_{F^i}^2 \lesssim \frac{k_{\max}}{k_{\min}}\left(|u-u_h|_{1,K,T_F^+\cup T_F^-}^2 + |u_h - I_h u_h|_{1,K,T_F^+\cup T_F^-}^2 + \epsilon(T_F^+\cup T_F^-)^2\right).$$

If the ghost edge F is not cut, the estimate is standard. Summing over all ghost edges and using the interpolation estimate $|u_h - I_h u_h|_{1,K,h} \lesssim \eta_\Gamma$ proved in [11], we obtain:

$$\left(\sum_{i=1}^2\sum_{F\in\mathcal{F}_g^i} \frac{h_F^2 k_i}{h_F^{\min}}\|[\![\partial_n(u-I_h u_h)]\!]\|_{F^i}^2\right)^{1/2} \lesssim C_h^\Gamma \frac{k_{\max}^{1/2}}{k_{\min}^{1/2}}\left(|u-u_h|_{1,K,h} + \eta_\Gamma + \epsilon(\Omega)\right). \tag{33}$$

According to (32), it remains to bound $\frac{h_F^2 k_i}{|F^i|}\|[\![\partial_n(u_{h,i}-I_h u_h)]\!]\|_{F^i}^2$. Since $[\![\nabla(u_{h,i}-I_h u_h)]\!]$ is constant on F^i by construction of $I_h u_h$, we first have

$$\frac{h_F^2 k_i}{|F^i|}\|[\![\partial_n(u_{h,i}-I_h u_h)]\!]\|_{F^i}^2 \leq h_F^2 \sum_{T\in\{T_F^+,T_F^-\}} k_i |\nabla(u_{h,i}-I_h u_h)_{|\tilde{T}^i}|^2,$$

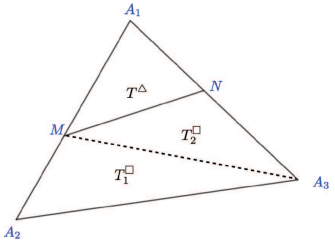

FIGURE 3. Element $T = \triangle A_1A_2A_3$ cut by $\Gamma_T = MN$ into three subtriangles.

where $\tilde{T}^i \subset \Omega^i$ denotes the sub-triangle of T containing F^i (*i.e.*, in the case T is cut into a triangular and a quadrilateral part, $\tilde{T}^i$ is one of the triangles T^{Δ}, $T_1^{\square}$ or $T_2^{\square}$ in Fig. 3; see Sect. 3.2 of [11] for more details). Note that only cut triangles contribute to the previous sum. Hence,

$$\sum_{i=1}^{2} \sum_{F \in \mathcal{F}_g^i} \frac{h_F^2 k_i}{|F^i|} \|[\![\partial_n (u_{h,i} - I_h u_h)]\!]\|_{F^i}^2 \leq \sum_{T \in \mathcal{T}_h^{\Gamma}} \sum_{\tilde{T} \in \{T^{\Delta}, T_1^{\square}, T_2^{\square}\}} h_T^2 |K^{1/2} \nabla (u_h - I_h u_h)_{|\tilde{T}}|^2.$$

Using the results of Lemmas 3.2–3.5 from [11], the right-hand side can be bounded by $\sum_{T \in \mathcal{T}_h^{\Gamma}} \frac{h_T}{h_T^{\min}} \tilde{\eta}_T^2$, which is further bounded by $(C_h^{\Gamma} \eta_{\Gamma})^2$. Combining this estimate with (32) and (33) yields:

$$\left(\sum_{i=1}^{2} j_i(u_{h,i}, u_{h,i}) \right)^{1/2} \lesssim C_h^{\Gamma} \frac{k_{\max}^{1/2}}{k_{\min}^{1/2}} \left(|u - u_h|_{1,K,h} + \eta_{\Gamma} + \epsilon(\Omega) \right).$$

The conclusion then follows from the reliability estimate (31) for $|u - u_h|_{1,K,h}$. □

The local efficiency is established with respect to the following norm of the error:

$$\|v_h\|_{h,\Delta_T}^2 = \sum_{i=1}^{2} \left(\|k_i^{1/2} \nabla v_{h,i}\|_{\Delta_T \cap \Omega^i}^2 + j_{i,\Delta_T}(v_{h,i}, v_{h,i}) \right) + \sum_{T \in \mathcal{T}_h^{\Gamma} \cap \Delta_T} \int_{\Gamma_T} \frac{k_{\Gamma}}{h_T} [v_h]^2 \, \mathrm{d}s,$$

where

$$\Delta_T = \bigcup_{N \in \mathcal{N}_T} \omega_N, \quad j_{i,\Delta_T}(v_{h,i}, v_{h,i}) := \sum_{T' \in \Delta_T} \sum_{F \in \mathcal{F}_g^i \cap \mathcal{F}_{T'}} h_F \int_F k_i [\![\partial_n v_{h,i}]\!]^2 \, \mathrm{d}s \quad (i = 1, 2).$$

We recall that $\mathcal{N}_T$ is the set of vertices of T and ω_N the set of triangles sharing the node N. It is also useful to introduce, for $F \in \mathcal{F}_h^{\Gamma}$, the notation $\Delta_F = \bigcup_{T,\, \partial T \supset F} \Delta_T$.

In the following, we state the local bound for each estimator η_T, $\tilde{\eta}_T$ and η_F, which are proved in [11]. The main difficulty lies in exhibiting the explicit dependence of the efficiency constants on the coefficients and on the interface geometry in the cut elements $T \in \mathcal{T}_h^{\Gamma}$. For theoretical reasons only, to establish the efficiency of η_T with the best constant, we make the following assumption.

Assumption 5.5. *For any $T \in \mathcal{T}_h^{\Gamma}$, there exist closed, regular shaped triangles $\tilde{T}^1 \subset \Omega^1, \tilde{T}^2 \subset \Omega^2$ such that they have Γ_T as a common side: $\tilde{T}^1 \cap \tilde{T}^2 = \Gamma_T$.*

Theorem 5.6. *Under Assumption 5.5, for any $T \in \mathcal{T}_h$ there exists a positive constant C_T such that*

$$\forall T \in \mathcal{T}_h, \quad \eta_T \lesssim C_T \left(\|u - u_h\|_{h,\Delta_T} + \epsilon(\Delta_T) \right), \tag{34}$$

with $C_T = 1$ if $T \in \mathcal{T}_h \backslash \mathcal{T}_h^{\Gamma}$ and $C_T = \max_{T' \in \Delta_T \cap \mathcal{T}_h^{\Gamma}} \frac{h_{T'}^{1/2}}{|\Gamma_{T'}|^{1/2}} \frac{k_{\max}^{3/2}}{k_{\min}^{3/2}}$ if $T \in \mathcal{T}_h^{\Gamma}$.

Remark 5.7. In the particular case where Assumption 5.5 might not hold, we can still prove cf. [20] a similar estimate to (34) but with an efficiency constant multiplied by $\sqrt{k_{\max}}/\sqrt{k_{\min}}$. It is worth noting that we have not noticed any influence of Assumption 5.5 in the numerical experiments, including the petal-shaped domain of Example 6.3 which presents a complex mesh/interface geometry.

Theorem 5.8. *Let $T \in \mathcal{T}_h^\Gamma$ and $F \in \mathcal{F}_h^\Gamma$. There exist positive constants $\tilde{C}_T$ and C_F such that*

$$\tilde{\eta}_T \lesssim \tilde{C}_T \|u - u_h\|_{h,T}, \qquad \eta_F \lesssim C_F \left(\|u - u_h\|_{h,\Delta_F} + \epsilon(\Delta_F) \right), \tag{35}$$

where $\tilde{C}_T = \frac{h_T}{\sqrt{h_T^{\min}|\Gamma_T|}}$ *and* $C_F = \max_{T \in \Delta_F \cap \mathcal{T}_h^\Gamma} \frac{h_T}{|\Gamma_T|} \frac{k_{\max}^{3/2}}{k_{\min}^{3/2}}$.

Theorems 5.6 and 5.8 assert the local efficiency, with explicit bounds of the efficiency constants. On a cut cell T and a cut edge F, C_T and C_F depend in theory on the ratio $k_{\max}/k_{\min}$; however, the numerical behavior of the global estimator appears to be quite robust with respect to this ratio, as shown in Figure 6 where we successfully tested a ratio of 10 000. On the cut elements, the three efficiency constants also depend on the ratio $h_T/|\Gamma_T|$, which is $O(1)$ for most elements and again does not seem to influence the numerical tests.

6. Numerical simulations

We present several numerical experiments to illustrate the theoretical results established in the previous sections. The numerical implementation is based on the open-source library FEniCS, along with the CutFEM library developed by Farina *et al.* [19], which is built based on FEniCS. Additional technical details regarding the challenges of implementing flux reconstruction on cut elements are provided in Appendix A.

For the stabilization parameters in the discrete problem, we set $\gamma = 10$ and $\gamma_g = 0.1$. The mesh refinement follows Dörfler's marking strategy [15], *i.e.*, we look for the set of elements $\mathcal{T}_h^m$ with minimal cardinality such that $\theta\eta(\mathcal{T}_h)^2 \leq \eta(\mathcal{T}_h^m)^2$. In the adaptive mesh refinement (AMR) procedure, the marking percent θ is set to be 35%, *i.e.*, the ordered elements that account for the top 35% of the total error estimator get refined. Although the reliability bound is established for the global error estimator $\eta + \eta_\Gamma$, we have observed in [11] that the numerical results obtained when using $\eta + \eta_\Gamma$ (and the corresponding error indicator $\eta_T + \tilde{\eta}_T + \sum_{F \in \mathcal{F}_h^\Gamma \cap \partial T} \eta_F$ for any $T \in \mathcal{T}_h$) in the AMR procedure are very similar to those obtained with the estimator η (and the indicator η_T) alone. The implementation of η_Γ is more technical, and its use is also more expensive; therefore, in the following tests we employ η_T as error indicator in the AMR procedure, and η as global error estimator.

In the following, we present three test cases. All convergence curves are displayed on a log–log scale.

Example 6.1 (Ellipse problem)**.** Let $\Omega = [-1, 1]^2$ and let Γ be the ellipse centered at the origin of equation $\rho = 1$, where $\rho = \sqrt{\frac{x^2}{a^2} + \frac{y^2}{b^2}}$ with $2a$ the width and $2b$ the height of the ellipse. Here, we take $a = \frac{\pi}{6.18}$ and $b = 1.5a$. The exact solution of (1) with $g = 0$ is given by

$$u(x, y) = \begin{cases} \dfrac{1}{k_1}\rho^p & \text{if } \rho \leq 1 \\ \dfrac{1}{k_2}\rho^p + \dfrac{1}{k_1} - \dfrac{1}{k_2} & \text{if } \rho > 1 \end{cases},$$

where $p = 5$. The diffusion coefficients in the two subdomains are $k_1 = 1$ (in the interior Ω^1 of the ellipse) and $k_2 = \mu k_1$, with $\mu > 0$ a parameter that we let vary in the numerical experiments.

We begin by testing the convergence rate of the flux reconstruction error between the exact flux $\sigma = K\nabla u$ and the recovered flux σ_h, that is $\|K^{-1/2}(\sigma - \sigma_h)\|_\Omega$. In this test, we set $\mu = 1$, so that $k_1 = k_2$, and consider a smooth solution $u \in H^2(\Omega)$. A uniform mesh refinement is applied. As shown in Figure 4, we observe the expected

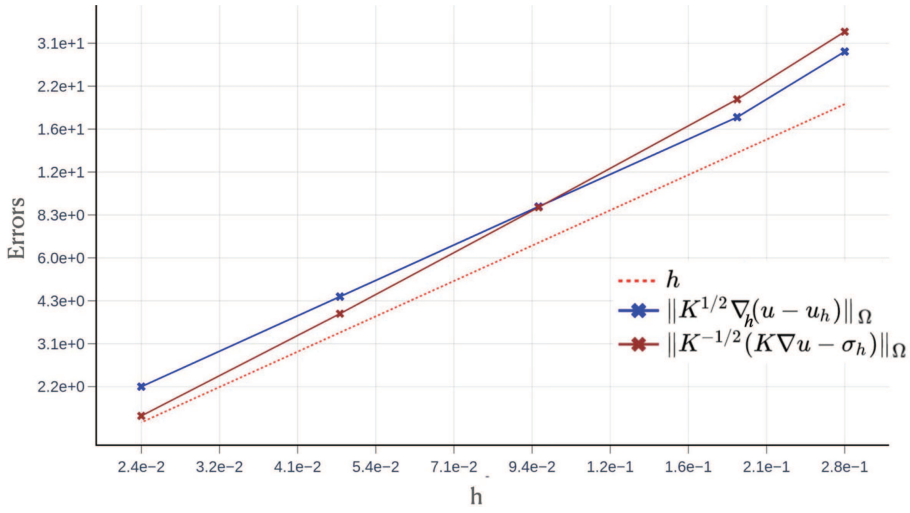

FIGURE 4. Example 6.1. Convergence of errors for $\mu = 1$ with uniform refinement.

optimal convergence rate $O(h) = O(N^{-1/2})$ for both the (weighted) energy norm error $\|K^{1/2}\nabla_h(u-u_h)\|_\Omega$ and the flux reconstruction error.

Figure 5 displays a sequence of adaptively refined meshes for $\mu = 100$, from the initial mesh to the final one at iteration 15. The AMR procedure is terminated when the total number of degrees of freedom N reaches 30 000. In Figure 6, we report the convergence results for different values of μ, ranging from 10 to 10 000.

In all cases, we observe the optimal convergence rate $O(N^{-1/2})$ for both the weighted H^1 semi-norm of the error and the global estimator η. The peaks observed in Figure 6 are likely caused by poor cuts induced by the interface, which result in large values of the ratio $h_T/\sqrt{h_T^{\min}|\Gamma_T|}$, and consequently in large theoretical efficiency constants C_T on the affected triangles (see also [11] for further details). In addition, the multiplicative factor $\mu^{3/2}$ appearing in C_T is also large. Nevertheless, the overall performance of the estimator is not affected, and the optimal convergence rate $O(N^{-1/2})$ is recovered for both the error and the estimator η. Table 1 shows the effectivity index for different values of μ during the last 8 refinement iterations. The previous numerical results confirm the robustness of the method with respect to the jump in the diffusion coefficients.

Example 6.2 (L-shaped problem)**.** We now consider the L-shaped domain test case, see for instance [3]. The domain is $\Omega = [-5,5]\times[-5,5]\backslash[0,5]\times[-5,0]$ and presents again an interface, the circle centered at the origin and of radius $\rho_0 = 2\sqrt{2}$. The exact solution is given in polar coordinates (ρ,θ) by:

$$u(\rho,\theta) = \begin{cases} \rho^{2/3}\sin(2\theta/3), & \text{if } \rho \le \rho_0 \\ \rho_0^{2/3}\sin(2\theta/3) + \dfrac{2}{3\mu}\rho_0^{-1/3}\sin(2\theta/3)(\rho-\rho_0) & \text{otherwise} \end{cases},$$

whereas the diffusion coefficient is equal to 1 inside the circle (in Ω^1) and to μ outside the circle (in Ω^2).

In order to validate the implementation of the $\mathcal{IRT}^0$-flux σ_h, we first consider the same diffusion coefficient in Ω, that is $\mu = 1$. Then the theory ensures that σ_h actually belongs to the standard Raviart–Thomas space on Ω, which is next confirmed numerically. The stopping criterion in the AMR procedure is again that N is less than 30 000. In Figure 7a we show the convergence rates for the estimator η based on σ_h, and the estimator $\eta_{RT^0} := \|K^{-1/2}(\tilde{\sigma}_h - K\nabla_h u_h)\|_\Omega$ based on a Raviart–Thomas flux $\tilde{\sigma}_h \in \mathcal{RT}^0(\mathcal{T}_h)$ which has the same degrees of freedom as σ_h, see also [20]. As we can notice, the two convergence curves for η and η_{RT^0} coincide. This

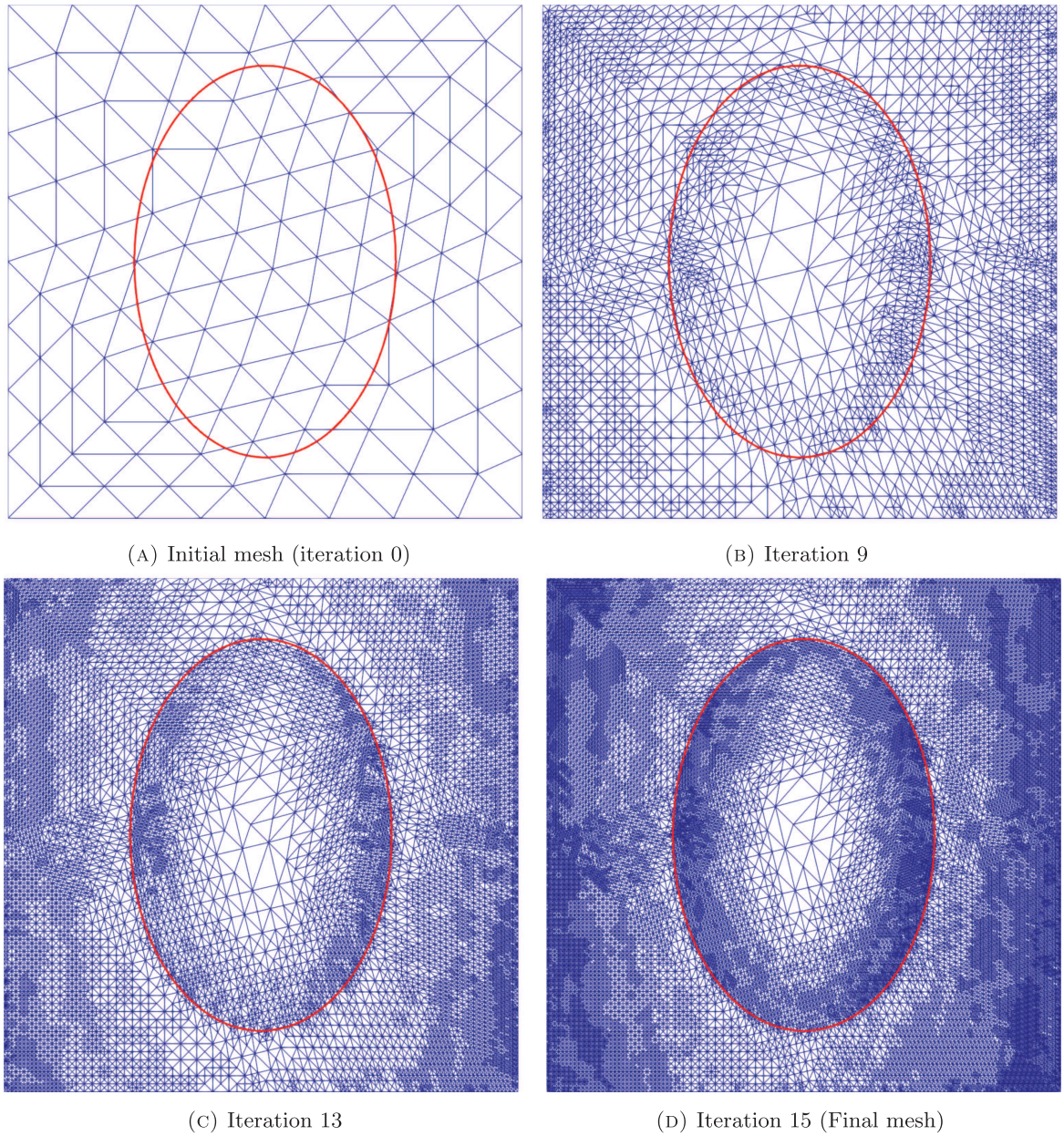

(A) Initial mesh (iteration 0)

(B) Iteration 9

(C) Iteration 13

(D) Iteration 15 (Final mesh)

FIGURE 5. Example 6.1. Sequence of adapted meshes for $\mu = 100$.

confirms that the flux σ_h, defined in the immersed Raviart–Thomas space, coincides with the flux defined in the standard Raviart–Thomas space, and thus validates the implementation of the space $\mathcal{IRT}^0$.

In Figure 7b we present the final adapted mesh, which shows that the refinement mainly takes place, as expected, near the re-entrant corner, where the solution is singular, and not particularly near the interface.

We take next $\mu = 5$. Figure 8 shows a sequence of adaptively refined meshes. In this test, the AMR procedure is stopped when N reaches 35 000. As expected, refinement occurs both near the interface and around the

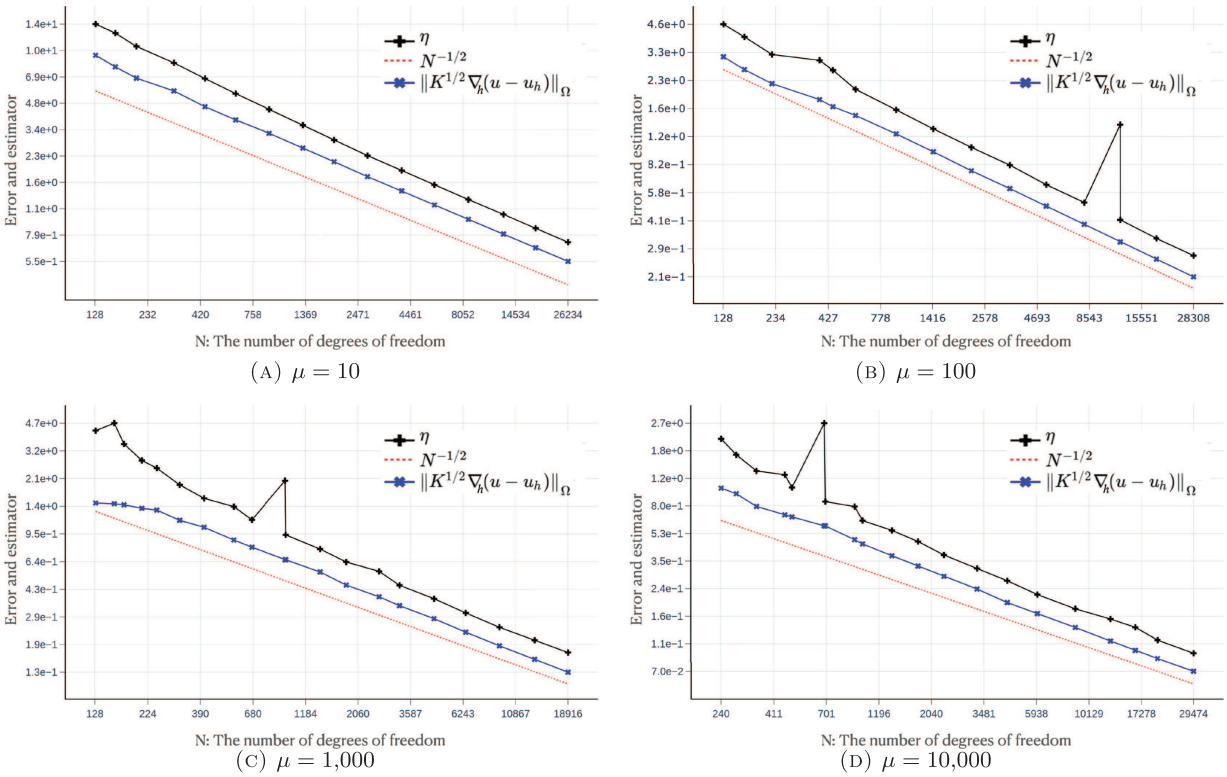

(A) $\mu = 10$ (B) $\mu = 100$

(C) $\mu = 1{,}000$ (D) $\mu = 10{,}000$

FIGURE 6. Example 6.1. Convergence of the error and the estimator η for different μ.

TABLE 1. Example 6.1. Effectivity index for different values of μ for the last 8 iterations.

$\mu = 10$	$\mu = 100$	$\mu = 1000$	$\mu = 10\,000$
1.346	1.354	1.396	1.353
1.334	1.342	1.444	1.378
1.323	1.373	1.342	1.323
1.315	1.321	1.335	1.315
1.311	1.317	1.321	1.381
1.308	1.309	1.308	1.404
1.306	1.303	1.318	1.312
1.299	1.335	1.328	1.303

re-entrant corner, where the solution exhibits a singularity. Figure 9 illustrates that both the weighted energy norm error and the *a posteriori* error estimator η converge optimally at the rate $O(N^{-1/2})$.

Example 6.3 (Petal-shaped problem)**.** Finally, we consider an interface problem characterized by a complex interface shape. The exact solution is described by a petal-shaped interface and is defined using the following level set function:

$$u(x,y) = \begin{cases} \phi(x,y), & \text{if } \phi(x,y) < 0 \\ \dfrac{1}{\mu}\phi(x,y), & \text{if } \phi(x,y) \geq 0, \end{cases} \qquad \forall (x,y) \in \Omega = [-1,1]^2$$

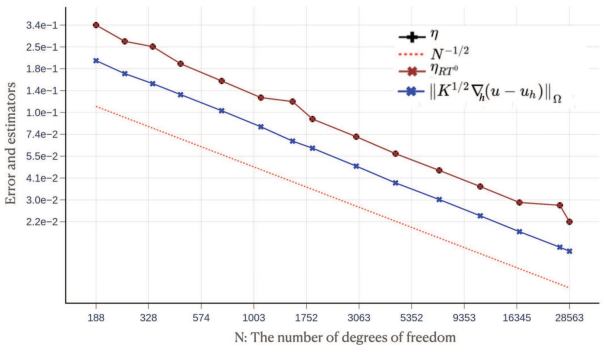

(A) Convergence rate for the error and the estimators η and η_{RT^0}

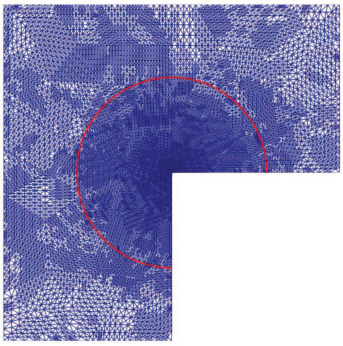

(B) Final mesh (iteration 14)

FIGURE 7. Example 6.2. Convergence of the error, η and η_{RT^0} (*left*) and final mesh (*right*) for $\mu = 1$.

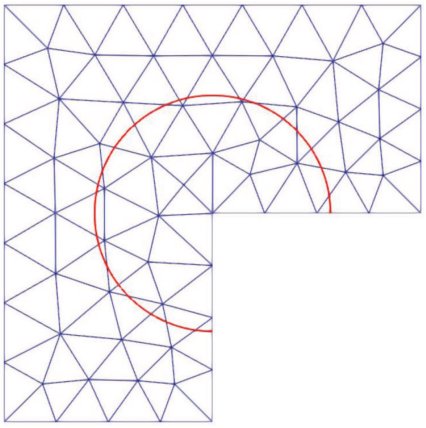

(A) Initial mesh (iteration 0)

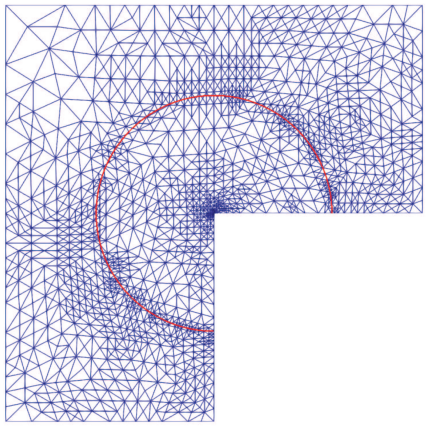

(B) Iteration 10

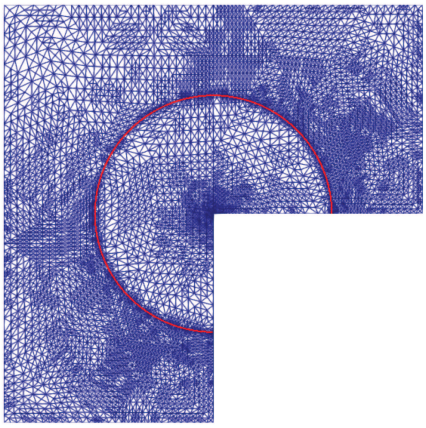

(C) Iteration 15

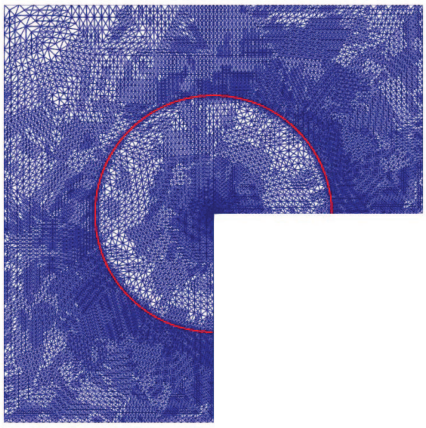

(D) Iteration 18 (final mesh)

FIGURE 8. Example 6.2. Sequence of adapted meshes for $\mu = 5$.

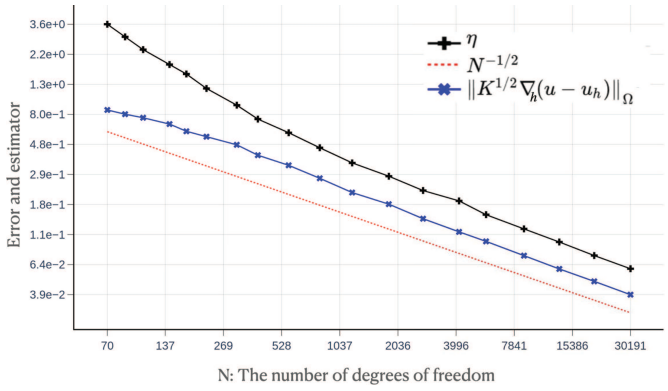

FIGURE 9. Example 6.2. Convergence of the error and the error estimator η for $\mu = 5$.

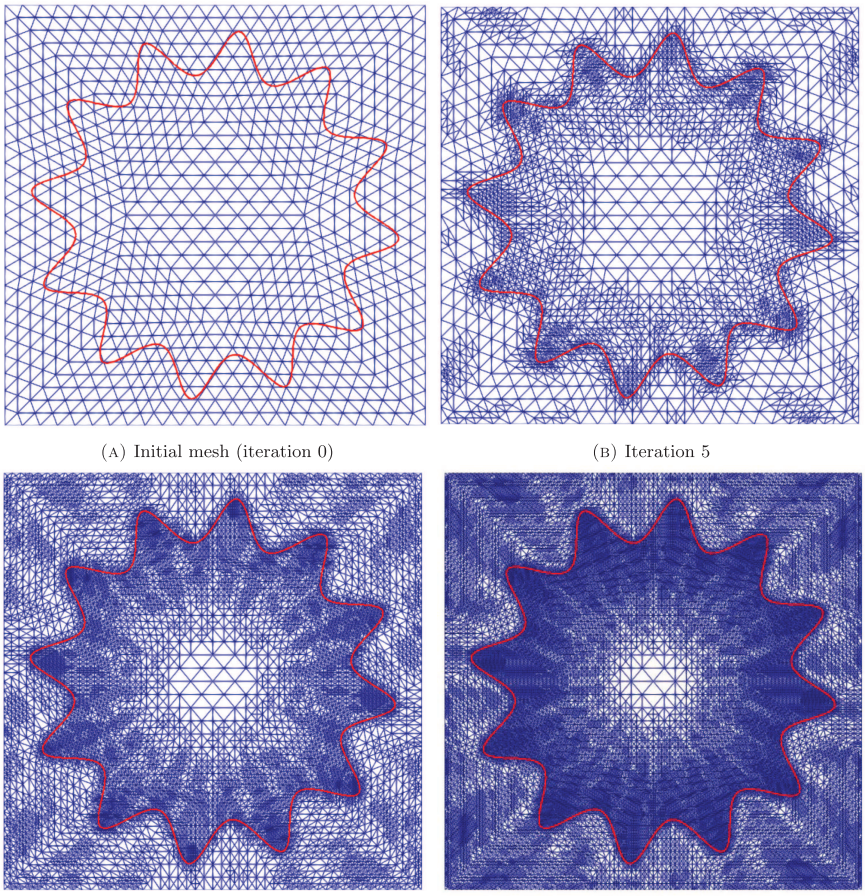

(A) Initial mesh (iteration 0)

(B) Iteration 5

(C) Iteration 8

(D) Iteration 10 (final mesh)

FIGURE 10. Example 6.3. Sequence of adapted meshes.

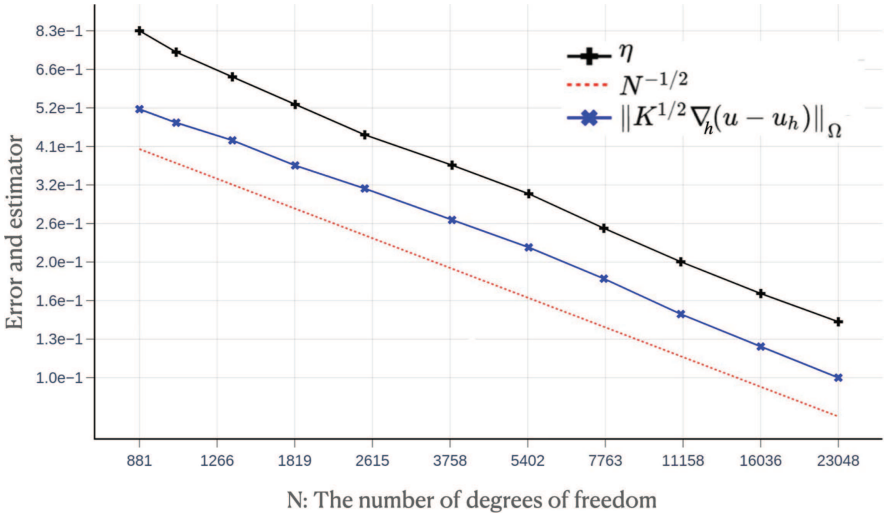

FIGURE 11. Example 6.3. Convergence of the error and the error estimator for $\mu = 100$.

with $\mu = 100$. Here, the level set function $\phi(x, y)$ is given by:

$$\phi(x,y) = (x^2+y^2)^2\left(1+0.5\sin\left(12\tan^{-1}\left(\frac{y}{x}\right)\right)\right) - 0.3.$$

The AMR stopping criterion we set for this example is that the total number of degrees of freedom N remains below 25 000. Figure 10 shows a sequence of adaptively refined meshes, where significant refinement is observed around the interface. This behavior is likely due to the higher curvature of the interface in this example.

The convergence plot of Figure 11 indicates the optimal rate decay $O(N^{-1/2})$ for both the error and the *a posteriori* error estimator η.

FUNDING

This project has received funding from the European Union's Horizon H2020 Research and Innovation under Marie Curie Grant Agreement N° 945416.

REFERENCES

[1] M. Ainsworth, A posteriori error estimation for discontinuous Galerkin finite element approximation. *SIAM J. Numer. Anal.* **45** (2007) 1777–1798.
[2] R. Becker, D. Capatina and R. Luce, Local flux reconstructions for standard finite element methods on triangular meshes. *SIAM J. Numer. Anal.* **54** (2016) 2684–2706.
[3] A. Bonito, R.A. Devore and R.H. Nochetto, Adaptive finite element methods for elliptic problems with discontinuous coefficients. *SIAM J. Numer. Anal.* **51** (2013) 3106–3134.
[4] D. Braess and J. Schöberl, Equilibrated residual error estimator for edge elements. *Math. Comput.* **77** (2008) 651–672.
[5] D. Braess, T. Fraunholz and R.H. Hoppe, An equilibrated a posteriori error estimator for the interior penalty discontinuous Galerkin method. *SIAM J. Numer. Anal.* **52** (2014) 2121–2136.
[6] F. Brezzi and M. Fortin, Mixed and Hybrid Finite Element Method. Springer-Verlag, New York (1991).
[7] E. Burman and P. Hansbo, Fictitious domain finite element methods using cut elements: II. A stabilized Nitsche method. *Appl. Numer. Math.* **62** (2012) 328–341.
[8] E. Burman, S. Claus, P. Hansbo, M.G. Larson and A. Massing, CutFEM: discretizing geometry and partial differential equations. *Int. J. Numer. Meth. Eng.* **104** (2015) 472–501.

[9] D. Cai, Z. Cai and S. Zhang, Robust equilibrated a posteriori error estimator for higher order finite element approximations to diffusion problems. *Numer. Math.* **144** (2020) 1–21.
[10] Z. Cai, C. He and S. Zhang, Generalized Prager–Synge identity and robust equilibrated error estimators for discontinuous elements. *J. Comput. Appl. Math.* **398** (2021) 113673.
[11] D. Capatina and A. Gouasmi, Elliptic interface problem approximated by CutFEM: II. A posteriori error analysis based on equilibrated fluxes. Preprint arXiv:2507.06740 (2025).
[12] D. Capatina and C. He, Flux recovery for Cut Finite Element Method and its application in a posteriori error estimation. *ESAIM: M2AN* **55** (2021) 2759–2784.
[13] D. Capatina, A. Gouasmi and C. He, Robust flux reconstruction and a posteriori error analysis for an elliptic problem with discontinuous coefficients. *J. Sci. Comput.* **98** (2024) 28.
[14] B. Cockburn, J. Gopalakrishnan and R. Lazarov, Unified hybridization of discontinuous Galerkin, mixed, and continuous Galerkin methods for second order elliptic problems. *SIAM J. Numer. Anal.* **47** (2009) 1319–1365.
[15] W. Dörfler, A convergent adaptive algorithm for Poisson's equation. *SIAM J. Numer. Anal.* **33** (1996) 1106–1124.
[16] A. Ern and M. Vohralìk, Polynomial-degree-robust a posteriori estimates in a unified setting for conforming, nonconforming, discontinuous Galerkin, and mixed discretizations. *SIAM J. Numer. Anal.* **53** (2015) 1058–1081.
[17] A. Ern, I. Mozolevski and L. Schuh, Accurate velocity reconstruction for discontinuous Galerkin approximations of two-phase porous media flows. *C. R. Math.* **347** (2009) 551–554.
[18] A. Ern, A.F. Stephansen and P. Zunino, A discontinuous Galerkin method with weighted averages for advection–diffusion equations with locally small and anisotropic diffusivity. *IMA J. Numer. Anal.* **29** (2009) 235–256.
[19] S. Farina, S. Claus, J.S. Hale, A. Skupin and S.P. Bordas, A cut finite element method for spatially resolved energy metabolism models in complex neuro-cell morphologies with minimal remeshing. *Adv. Model. Simul. Eng. Sci.* **8** (2021) 1–32.
[20] A. Gouasmi, *Numerical flux reconstruction for an interface problem and application to a posteriori error analysis*. Ph.D. thesis, Université de Pau et des Pays de l'Adour (2024).
[21] R. Guo, Solving parabolic moving interface problems with dynamical immersed spaces on unfitted meshes: fully discrete analysis. *SIAM J. Numer. Anal.* **59** (2021) 797–828.
[22] J. Haifeng, An immersed Raviart–Thomas mixed finite element method for elliptic interface problems on unfitted meshes. *J. Sci. Comput.* **91** (2022) 66.
[23] Z. Li, The immersed interface method using a finite element formulation. *Appl. Numer. Math.* **27** (1998) 253–267.
[24] J. Nitsche, Uber ein Variationsprinzip zur Löosung von Dirichlet-Problemen bei Verwendung von Teilräumen, die keinen Randbedingungen unterworfen sind. Abh. Math. Sem. Univ. Hamburg (1971).
[25] L.H. Odsaeter, M.F. Wheeler, T. Kvamsdal and M.G. Larson, Postprocessing of nonconservative flux for compatibility with transport in heterogeneous media. *Comput. Methods Appl. Mech. Eng.* **315** (2017) 799–830.
[26] P.-A. Raviart and J.-M. Thomas, A mixed finite element method for second order elliptic problems, in Mathematical Aspects of the Finite Element Method. *Lect. Notes in Math.* Vol. 606. Springer-Verlag, Berlin (1977).
[27] R. Verfürth, A note on constant-free a posteriori error estimates. *SIAM J. Numer. Anal.* **47** (2009) 3180–3194.
[28] M. Vohralìk, Guaranteed and fully robust a posteriori error estimates for conforming discretizations of diffusion problems with discontinuous coefficients. *J. Sci. Comput.* **46** (2011) 397–438.
[29] M. Vohralìk and M.F. Wheeler, A posteriori error estimates, stopping criteria, and adaptivity for two-phase flows. *Comput. Geosci.* **17** (2013) 789–812.

Appendix A. Numerical implementation of the flux on cut elements

Let $T \in \mathcal{T}_h^\Gamma$ and $\sigma_h \in \mathcal{IRT}^0(T)$. There exists a couple $(\sigma_{h,1}, \sigma_{h,2}) \in \mathcal{RT}^0(T) \times \mathcal{RT}^0(T)$ such that

$$[\sigma_h \cdot n_\Gamma] = \sigma_{h,1} \cdot n_\Gamma - \sigma_{h,2} \cdot n_\Gamma = 0, \tag{A.1}$$

$$[K^{-1}\sigma_h \cdot t_\Gamma](x_\Gamma) = k_1^{-1}\sigma_{h,1}(x_\Gamma) \cdot t_\Gamma - k_2^{-1}\sigma_{h,2}(x_\Gamma) \cdot t_\Gamma = 0, \tag{A.2}$$

$$\operatorname{div} \sigma_{h,1} = \operatorname{div} \sigma_{h,2}. \tag{A.3}$$

The idea for the implementation of the immersed Raviart–Thomas space is to express the degrees of freedom of $\sigma_{h,1}$ and $\sigma_{h,2}$ in terms of those of σ_h. Thus, instead of implementing the flux $\sigma_h \in \mathcal{IRT}^0(\mathcal{T}_h)$, which is challenging due to its discontinuity across cut edges and the available data types in FEniCS, we have chosen to implement the two functions $\sigma_{h,1}$ and $\sigma_{h,2}$, which belong to the standard Raviart–Thomas space.

We recall that the local degrees of freedom of $\mathcal{RT}^0(T)$ are given in (21) and that the basis function associated to the edge $F_j \in \partial T$ is given by

$$\Lambda_{T,j}(x) = \frac{|F_j|}{2|T|}\overrightarrow{A_j x}, \quad 1 \le j \le 3,$$

where A_j is the vertex of T opposite to F_j. One further has the unique decomposition:

$$\sigma_{h,i} = \sum_{j=1}^{3} N_{T,j}(\sigma_{h,i})\Lambda_{T,j} \quad (1 \le i \le 2).$$

Since $\sigma_{h,i} \cdot n_\Gamma \in P^0(\Gamma_T)$ for $i \in \{1,2\}$, condition (A.1) can be written as

$$\begin{gathered} \sigma_{h,1}(x_\Gamma) \cdot n_\Gamma - \sigma_{h,2}(x_\Gamma) \cdot n_\Gamma = 0 \iff \\ \sum_{j=1}^{3} |F_j| \overrightarrow{A_j x_\Gamma} \cdot n_\Gamma (N_{T,j}(\sigma_{h,1}) - N_{T,j}(\sigma_{h,2})) = 0, \end{gathered} \tag{A.4}$$

while (A.2) yields

$$\sum_{j=1}^{3} |F_j| \overrightarrow{A_j x_\Gamma} \cdot t_\Gamma (k_1^{-1} N_{T,j}(\sigma_{h,1}) - k_2^{-1} N_{T,j}(\sigma_{h,2})) = 0. \tag{A.5}$$

Since $\operatorname{div} \sigma_{h,i} \in P^0(T)$ for $i \in \{1,2\}$, condition (A.3) is equivalent to $\int_T \operatorname{div}(\sigma_{h,1} - \sigma_{h,2})\,\mathrm{d}x = 0$. Integration by parts further yields

$$\sum_{j=1}^{3} |F_j| (N_{T,j}(\sigma_{h,1}) - N_{T,j}(\sigma_{h,2})) = 0. \tag{A.6}$$

Denoting, for $1 \le i \le 2$ and $1 \le j \le 3$, the unknowns by $x_j^i := |F_j| N_{T,j}(\sigma_{h,i})$ and the coefficients by $\alpha_j := \overrightarrow{A_j x_\Gamma} \cdot n_\Gamma$ and $\beta_j := \overrightarrow{A_j x_\Gamma} \cdot t_\Gamma$, conditions (A.4), (A.5) and (A.6) translate into the following linear system:

$$\begin{cases} \alpha_1 x_1^1 + \alpha_2 x_2^1 + \alpha_3 x_3^1 + \alpha_1 x_1^2 + \alpha_2 x_2^2 + \alpha_3 x_3^2 = 0 \\ k_1^{-1}\beta_1 x_1^1 + k_1^{-1}\beta_2 x_2^1 + k_1^{-1}\beta_3 x_3^1 + k_2^{-1}\beta_1 x_1^2 + k_2^{-1}\beta_2 x_2^2 + k_2^{-1}\beta_3 x_3^2 = 0 \\ x_1^1 + x_2^1 + x_3^1 - x_1^2 - x_2^2 - x_3^2 = 0. \end{cases} \tag{A.7}$$

Assume now, without loss of generality, that the non-cut edge of T is F_1. Then one has that

$$N_{T,1}(\sigma_h) = \begin{cases} N_{T,1}(\sigma_{h,1}) & \text{if } F_1 \subset \Omega^1 \\ N_{T,1}(\sigma_{h,2}) & \text{if } F_1 \subset \Omega^2. \end{cases} \tag{A.8}$$

Furthermore, for any $j \in \{2,3\}$, one has

$$|F_j| N_{T,j}(\sigma_h) = \int_{F_j^1} \sigma_{h,1} \cdot n_T \, \mathrm{d}s + \int_{F_j^2} \sigma_{h,2} \cdot n_T \, \mathrm{d}s = \frac{|F_j^1|}{|F_j|} x_j^1 + \frac{|F_j^2|}{|F_j|} x_j^2. \tag{A.9}$$

Assuming that $F_1 \subset \Omega^1$ and denoting the coefficients $\omega_j^i := \frac{|F_j^i|}{|F_j|}$, for $2 \le j \le 3$ and $1 \le i \le 2$, equations (A.8) and (A.9) can be equivalently written as follows:

$$\begin{cases} x_1^1 = |F_1| N_{T,1}(\sigma_h) \\ \omega_2^1 x_2^1 + \omega_2^2 x_2^2 = |F_2| N_{T,2}(\sigma_h) \\ \omega_3^1 x_3^1 + \omega_3^2 x_3^2 = |F_3| N_{T,3}(\sigma_h). \end{cases} \tag{A.10}$$

Finally, gathering together (A.7) and (A.10), we obtain the linear system:

$$\begin{pmatrix} 1 & 0 & 0 & 0 & 0 & 0 \\ 0 & \omega_2^1 & 0 & 0 & \omega_2^2 & 0 \\ 0 & 0 & \omega_3^1 & 0 & 0 & \omega_3^2 \\ 1 & 1 & 1 & -1 & -1 & -1 \\ \alpha_1 & \alpha_2 & \alpha_3 & -\alpha_1 & -\alpha_2 & -\alpha_3 \\ k_1^{-1}\beta_1 & k_1^{-1}\beta_2 & k_1^{-1}\beta_3 & -k_2^{-1}\beta_1 & -k_2^{-1}\beta_2 & -k_2^{-1}\beta_3 \end{pmatrix} \begin{pmatrix} x_1^1 \\ x_2^1 \\ x_3^1 \\ x_1^2 \\ x_2^2 \\ x_3^2 \end{pmatrix} = \begin{pmatrix} b_1 \\ b_2 \\ b_3 \\ 0 \\ 0 \\ 0 \end{pmatrix} \tag{A.11}$$

where the right-hand side term is known, thanks to the definition (22) and (23) of the flux: $b_j = |F_j| N_{T,j}(\sigma_h)$ for $1 \le j \le 3$. Solving (A.11) allows to compute $N_{T,j}(\sigma_{h,i})$ for $1 \le j \le 3$ and $1 \le i \le 2$, and hence substitute σ_h by two Raviart–Thomas functions.